substance: boron compounds with lanthanides
property: properties of lanthanide hexaborides: SmB_6

Structure, chemical bond

lattice parameters
(in Å)

a	4.1336(2)	*T* = 300 K	X-ray diffraction	91T
	4.13319(3)	*T* = 300 K	$^{154}Sm^{11}B_6$, X-ray diffraction	93T
	4.13173(3)	*T* = 153 K	(occupancy of B for 23, 153 and 300 K	
	4.13302(3)	*T* = 23 K	= 91.5(5) %)	
	4.1304	*T* = 300 K	see also [56P]	71N1, 77E, 79G

For NMR studies of valence fluctuations, see [81T]; for NMR studies and spin/charge fluctuations, see [81P].

lattice parameters in the homogeneity range (*T* = 304 K)

	a (in Å)	*V* (in Å^3)		
SmB_6	4.1334(2)	70.62(1)	X-ray diffraction	83P
$Sm_{0.97}B_6$	4.1317(2)	70.53(1)	prepared from SmB_6 master alloy	
$Sm_{0.94}B_6$	4.1301(2)	70.45(1)	prepared from $Sm_{0.94}B_6$ master alloy	
$Sm_{0.90}B_6$	4.1280(2)	70.35(1)		
$Sm_{0.89}B_6$	4.1272(1)	70.30(1)		
$Sm_{0.81}B_6$	4.1281(1)	70.35(1)		
$Sm_{0.79}B_6$	4.1272(2)	70.30(1)		
$Sm_{0.71}B_6$	4.1277(1)	70.33(1)		

Differences of the structural data relative to those in [71N1] are discussed in [83P].

Homogeneity range of SmB_6 from $Sm_{0.7}B_6$ to SmB_6 [90K1].

Theoretical consideration of the preparation of lanthanide hexaborides, in particular SmB_6 with different Sm and B isotopes, by the reduction of metal oxides in the aluminium melt in [94G].

Synthesis and properties of SmB_6 in [59S].

Preparation of single crystals, powder neutron diffraction and X-ray single-crystal diffractometry studies [91T].

Valence of samarium in isostructural phases SmB_6 and $Sm_{0.8}B_6$ [83A2].

Growth and crystal data for preparation by high temperature solution growth [84L] and references therein.

Isotopic engineering of zero-matrix samarium hexaboride: results of high-resolution powder diffraction and X-ray single-crystal diffractometry studies [91T].

NMR-determined temperature dependence of the nuclear relaxation rate of various samples prepared by different methods in Fig. 1 [83T].

Electronic properties

From detailed neutron scattering studies was concluded that the characteristic features of the IV ground state wave function of Sm are the existence of strongly broadened high-energy excitations originating from former single-ion states f^5 and f^6 and a low-energy narrow excitation, which is specific for the quantum mixed state of intermediate-valence ions [93A2].

Calculated electronic band structure in Fig. 2 [83F].

Energy band scheme based on experimental data in Fig. 3 [99D, 99G].

In the electronic structure of SmB_6 a narrow f band with large Coulomb interaction, a wide d band with negligible interactions, f–d hybridization, Coulomb, and exchange interactions are assumed. Since in the case of SmB_6 the two bands contain an even integral number of electrons per rare earth ion, intersite correlations profoundly affect states near the Fermi energy and lead to a small insulating gap [79M]. See also [70C, 71N2, 73M, 77O].

For Sm $M_{4,5}$ spectra of SmB_6, see [82A]; for Sm Lγ_1 emission spectra in SmB_6, see [82T]; for BK spectra in SmB_6, see [82O].

energy gap
(in meV)

E_g	0		calculated (semimetal)	83F
	5		el. cond.(Fig. 6)	77E
	2.3		electrical conductivity	69M1
	~5			84K
	4.4		el. cond.	83B
	1.8...2.7		el. cond.	87W
	14		neutron scattering	93A3, 95A
	7	T = 10...49 K	electron tunneling	98A
	19(2)	T = 3...20 K	interband, dynamical conductivity (see Figs.3, 4)	99D, 99G
E_d	3	T = 3...20 K	donor level; dynam. cond. (see Figs. 3, 5)	99G

Electron-tunneling studies compared with CeB_6, EuB_6 SrB_6 in [98A].

SmB_6 possesses a magnetic moment like CeB_6 and EuB_6 but in contrast to SrB_6 [98A].

Pressure dependence of the energy gap derived from electrical conductivity in Fig. 7 [83B].

The properties of borides of metals with mixed valence [79P].

Electron energy loss function in [81S].

Calculated interband density of states in Fig. 8 [87W].

Calculated densities of states: see Fig. 43 [79M2].

Interaction of 4f electrons with the lattice in the mixed valence model [85P1].

B K emission and absorption spectrum (compared with LaB_6 and EuB_6) [82O].

Influence of the mixed-valences state on the magnetic excitation spectrum of SmB_6-based compounds [97A].

Impurities and defects

On the influence of defects and impurity atoms on the properties of rare-earth hexaborides with mixed valency: Variation of the lattice parameters, when La, Eu, Gd substitute for Sm in Fig. 9, variation of the effective valence of the Sm atoms for Eu, La, Yb, Dy, Ba, Gd atoms substituting for Sm in Fig. 10 [81F, 87P].

The influence of Sm vacancies is discussed in [77K] and [78A].

Effect of vacancies on the lattice parameter and on the valence state of samarium in Sm_xB_6 in Fig. 11 [82K].

NMR study of the mixed valent compound of SmB_6 with La and Yb substitution in [83T].

Temperature dependence of the electrical resistivity of SmB_6 with Ba, La, and Gd atoms substituted for Sm in Fig. 12 [84K].

Temperature dependence of lattice parameters of $Sm_xMe_{1-x}B_6$ (Me = Ca, La) in Fig. 13 [91A].

Dependence of the electrical resistivity of $Sm_xLa_{1-x}B_6$ and $Sm_xGd_{1-x}B_6$ on the concentration of Sm atoms compared with the variation of the lattice parameters in Fig. 14 [84K].

Lattice properties

Temperature dependence of the thermal expansion $\Delta l/l$ and the derived expansion coefficient in Fig. 15 [87W].

Temperature dependence of the lattice parameters in Fig. 16 [93T].

Isotropic thermal parameters of the Sm atom and anisotropic thermal parameters of the B atom in $^{154}Sm^{11}B_6$ in Fig. 17 [93T].

Thermal vibrations and static displacement of atoms in samarium hexaboride (compared with neodymium hexaboride) crystals in [94T].

Temperature dependence of the effective Debye temperature in Fig. 18 [93T].

Phonon dispersion curves of SmB_6 experimentally determined by neutron scattering compared with calculated curves for LaB_6 in Fig. 19 [91A].

phonon wavenumbers
(in cm^{-1})

FT Raman	Raman	Neutron scattering
[97S]	[81M]	[93A2]
1556		
1495		
1452		
1414		
1368		
1333	1290	
1233		1223
1133	1170	1149
1099		
983		
872		863
		812
645	734	715
615		
572		
547		543
491		
321		
288		274
237		
118	172	158
83		74

Low frequency part of the FT Raman spectrum [97S] compared with the phonon branches obtained on $^{154}Sm^{11}B_6$ by inelastic neutron scattering [91A, 93A2] in Fig. 20.

Raman spectra and frequencies see also **properties of lanthanide hexaborides: YbB_6** (Optical prop.)

Spectral range of phonon excitations (FT Raman spectrum [97S]), conventionally measured Raman spectrum [81M], inelastic neutron scattering [93A2] in Fig. 21.

See also neutron scattering under Further properties

elastic constants

(in 10^{11} dyn cm^{-2})

c_{11}	41.7	T = 300 K	lattice dynamics	85S1
c_{12}	–6.7			
c_{44}	7.8			83K
c_{bulk}	9.4			

Transport properties

dc electrical conductivity

σ	$5.3 \cdot 10^3\ \Omega^{-1}cm^{-1}$	T = 300 K		84K
	$3.3 \cdot 10^3\ \Omega^{-1}cm^{-1}$	T = 300 K		81K

Temperature dependence of the electrical conductivity of monocrystalline and polycrystalline SmB_6 in Fig. 22 [79A, 81K, 82F, 84K].

Temperature dependence of the dc conductivity and evaluation in Fig. 23 [99G].

Temperature dependence of the resistance for different pressures in Fig. 24 [83B]; see also [83A2, 89S].

Pressure dependence of the resistivity of SmB_6 compared with LaB_6 in [89S].

Pressure dependence of the electrical resistivity of LaB_6, SmB_6, YbB_6 and EuB_6 in Fig. 25 [81K, 91S1].

resistivity

(in Ω cm)

			films of different thicknesses	
ρ	$3.0 \cdot 10^{-4}$	T = 300 K	d = 1.00 μm; a = 4.14 Å	90K2
	$2.3 \cdot 10^{-4}$		d = 0.70 μm; a = 4.08 Å	
	$1.7 \cdot 10^{-4}$		d = 0.27 μm; a = 4.07 Å	
	$1.5 \cdot 10^{-4}$		d = 0.15 μm; a = 4.05 Å	

For temperature dependence see [90K2].

resistivity (further data)

ρ	3...10·10^{-4} Ω cm	T = 300 K	see Figs. 6, 26; see also [70Y]	75A, 78A, 75S, 69P, 80L
	1.2·10^{-3} Ω cm	T = 300 K,230 Hz		79A
	1.7·10^{-4} Ω cm	T = 10 K		77E
	3·10^{-2} Ω cm	T = 10 K		71N2
	3 Ω cm	T = 4 K,230 Hz	For temperature dependence, see Fig. 27	76A

temperature coefficient of ρ

$(1/\rho)\mathrm{d}\rho/\mathrm{d}T$	– 42·10^{-2} K^{-1}	T = 300 K		75S

pressure dependence of ρ

$(\mathrm{d}\log\rho/\mathrm{d}p)_{p=0}$	– 25·10^{-3} kbar^{-1}	T = 300 K		80L

parameters of charge carriers [99G]
(calculated on the basis of the measured Hall constant R_H and on the relaxation frequency and plasma frequency obtained from the submillimeter conductivity and permittivity spectra in Fig. 4)

T [K]	R_H [cm^{3}C^{-1}]	γ [cm^{-1}]	μ_H [cm^{2}V^{-1}s^{-1}]	n [10^{19} cm^{-3}]	m^*/m_0
14	–0.35	3	80	1.8	110
16	–0.19	4.3	66	3.2	94
18	–0.117	5.5	52	5.7	94

dynamical conductivity

Dielectric response in the millimeter wave range, dynamical conductivity and permittivity spectra in Fig. 4 [99D].

Temperature dependence of the plasma frequency of free carriers in Fig. 5.

thermoelectric power
(in μV K^{-1})

S	12.5	T = 300 K	different surrounding media	89S
	7.5			
	11.7	T = 310 °C	largely linear T-dependence	59S
	13.6	T = 550 °C	for T dep. see Ref.	
	– 320	$T \approx$ 10 K		77E
	+ 8.4	$T \approx$ 300 K		69P, 75S, 62S

For temperature dependence of the thermoelectric power see Fig. 28.

Pressure dependence of the thermoelectric power of monocrystals in Fig. 29 [89S].

Hall coefficient
(in cm^3C^{-1})

R_H	–0.735	T = 4.2 K		73S3
	–0.307	T = 11.4 K		
	$-9.3\cdot10^{-3}$	T = 70 K		
	$+2.7\cdot10^{-4}$	T = 293 K		

Temperature dependence of Hall coefficient in Fig. 30 [81K].

Temperature dependence of Hall coefficient also in [79A].

Magnetoresistance $\Delta\rho/\rho_0$ for T =1.56 and 4.2 K up to B = 5.5 T in Fig. 31 [84K, 83A1].

mobility

μ_H	– 20 cm^2/V s	T = 10 K	see Fig. 26	71N2

electron mobility
(in $cm^2V^{-1}s^{-1}$)

μ	$2.79\cdot10^{-4}$	T = 300 K	estimated	79A
	1.7	T = 4.2 K	ρ = 0.21 Ω cm	73S3
	31.3	T = 11.4 K	$\rho = 2.3\cdot10^{-2}$ Ω cm	
	20.7	T = 70 K	$\rho = 2.3\cdot10^{-2}$ Ω cm	
	0.85	T = 293 K	$\rho = 6.0\cdot10^{-4}$ Ω cm	

carrier concentration
(in cm^{-3})

n	$2.08\cdot10^{17}$	T = 4 K	estimated upper bound of n	79A
p	$5.2\cdot10^{17}$	T = 4 K	estimated upper bound of p	
n	$9\cdot10^{21}$	T = 300 K	estimated	
n	$8\cdot10^{20}$	T = 4.2 K	ρ = 0.21 Ω cm	73S3
	$2\cdot10^{19}$	T = 11.4 K	$\rho = 2.3\cdot10^{-2}$ Ω cm	
	$6.7\cdot10^{20}$	T = 70 K	$\rho = 6.0\cdot10^{-4}$ Ω cm	
p	$2.5\cdot10^{22}$	T = 293 K	$\rho = 2.5\cdot10^{-4}$ Ω cm	
n	$5\cdot10^{17}$	T = 4 K	estimated maximum concentration	87W
	$8.5\cdot10^{21}$		estimated for valency 2.6 without gap	

For Hall coefficient, see Fig. 32, see also [71N2].

For electrical properties of SmB_6, see also [81K].

For resistivity. thermoelectric power, magnetic susceptibility, Hall constant, thermal conductivity of SmB_6 see also [73S3].

Optical properties

Real part of the optical conductivity (4 K and 300 K) in Fig. 33 [87W].

Reflectivity spectrum in Fig. 34 [81S].

Dielectric function up to 42 eV in Fig. 35 [81S].

Reflectivity and dielectric function see also **properties of lanthanide hexaborides: YbB_6** (Optical prop.)

For the high energy reflectivity spectrum and the dielectric function see also [83F].

reflectivity minimum
(energy in eV)

R_{min}	0.12	T = 300 K		81S
E (R_{min})	1.8			
E (R_{min})	1.957	T = 300 K	single crystal after annealing	94K1
	1.957		powder	

FIR reflectivity spectrum of SmB_6 in Fig. 36 [87W].

emissivity

ε	0.75	T = 900 °C	linear T-dependence	59S
	0.67	T = 1600 °C		

Further properties

density

d	5.076 g cm^{-3}	T = 300 K	X-ray	75S
	4.79 g cm^{-3}		pycnometric	75S

magnetic susceptibility

Temperature dependence of the magnetic susceptibility in Fig. 37 [87W].

thermal conductivity

Temperature dependence of thermal conductivity of mono- and polycrystalline SmB_6 in [84K].

Thermal conductivity of single and polycrystals in Fig. 38 [82F].

linear thermal expansion coefficient

α	$6.5 \cdot 10^{-6}$ K^{-1}	T = 300 K		75S

heat capacity

Temperature dependence of C_p in [85P1, 78R].

Calculation formula for the low temperature electron heat capacity depending on the pecularities of the electron density of states distribution in SmB_6 and EuB_6 [87A].

See also Fig. 39

Debye temperature
(in K)

Θ_D	182	T < 5 K	low temperature heat capacity	91S2
	212	T = 0...10 K	specific heat	70E
	250	T = 0...10 K	specific heat	69M2
	200			79T
	275			85P1
	217			86G
	404	T ~ 300 K	ultrasonic method	77T
	468	low temp.	el. resistivity	77T
	491	T = 300 K	X-ray diffraction	87K2, 87K1
	720		elastic constants	73D
	245	T = 4.2 ... 300 K	electrical conductivity	76T
	710	T = 300 K	X-ray	73D
	660	T = 1000 K		
	417	T = 300 K	metal sublattice; X-ray	87K1
	732		boron sublattice, X-ray	
	373		lattice dynamics	85S2
	518 K	T < 300 K	$^{154}Sm^{11}B_6$, average, for T-dep. see ref. (corrected for static displacement)	94T

Characteristic Einstein temperatures of Sm in relation to other RE atom in the hexaborides in Fig. 40 [94K2].

Characteristic Einstein frequencies also in [94C].

melting point

T_m	2580 °C			96G
	2540°C			75S
	1810°C			
	2400°C			
	> 2500°C			80H

microhardness
(in kg mm^{-2})

H_K	1920	T = 300 K	cube, average value; load 50 g	96G
	1540		rhombododecahedron, average value; load 50 g	
	1790		(100) face	94C

High temperature hardness of single crystals of LaB_6, CeB_6, PrB_6, NdB_6 and SmB_6 [99O].

entropy

S	97.9(42) J mol^{-1}K^{-1}			86B

neutron scattering

Lattice and magnetic excitations in SmB_6 [93A1].

observed maxima of neutron scattering

maxima attributed to phonons (E in meV):

$E(S_{max})$	~10	T = 20 K	E_0 = 60 meV, Φ = 5°	93A2
	~14			
	~25			

maxima attributed to magnetic interactions:

$E(S_{max})$	~40	T = 20 K	E_0 = 300 meV, Φ = 5°	93A2
	~120			

Neutron scattering spectra in Fig. 41 and Fig. 42 [93A3].

work function

Φ	4. eV			75S
	4.30(5) eV	T = 300 K	For temperature dependence at high temperatures. see original paper.	79S
	4.24(7) eV			80F

emissivity at 655 mn

ε	0.68			75S

microhardness

H	2500 kg mm^{-2}	T = 300 K	hardness not specified	75S

magnetic moment

p_{eff}	2.52 μ_B	effective magnetic moment		75S

magnetic susceptibility

χ_m	1810·10^{-6} cm^3 mol^{-1}	T = 300 K	χ_m in CGS-emu	75S

molar susceptibility of SmB_6: Fig. 44 [69M1, 71N2].

References:

56P Post, B., Moskowitz, D., Glaser, F. W.: J. Am. Chem. Soc. 78 (1956) 1800.

59S Samsonov, G.V., Shravlev, N.N., Paderno, Yu.B., Melik-Adamyai, V.R.: Kristallografiya 4 (1959) 538 (in Russian).

62S Samsonov, G. V., Vainshtein, E. Y., Paderno, Y. B.: Fiz. Metal. Metallov. 13 (1962) 764

69M1 Menth, H., Buehler, E., Geballe, T. H.: Phys. Rev. Lett. 22 (1969) 295.

69M2 Mercurio, J.P., Etourneau, J., Naslain, R., Hagenmuller, P.: C. R. Acad. Sci. (Paris) B 268 (1969) 1766.

69P Paderno, Yu. B., et al.: Poroshk. Metall. Acad. NAUK Ukr. SSR 10 (1969) 55.

70C Cohen, R.L., Eibschutz, M., West, K.:Phys. Rev. Lett. 24 (1970) 383.

70E Etourneau, J., Mercurio, J.P., Naslain, R., Hagenmuller, P.: J. Solid State Chem. 2 (1970) 332.

70Y Yajima, S., Nuhara, K.: Proc. 9th Rare Earth Research Conf, US Dept. of Commerce, 1970, p. 598.

71N1 Nuhara, K.: Bull Chem. Soc. Jpn. 44 (1971) 963.

71N2 Nickerson, J. C., White, R. M., Lee, K. N., Bachmann, R., Geballe, T. H., Hull, G. W. Jr.: Phys. Rev. B 3 (1971) 2030.

72H Hacker, H.: J. Magn. Reson. 8 (1972) 175.

73D Dutchak, Ya.I., Fedishin, Ya.I., Paderno, Yu.B., Vadets, D.I.: Izv. V.U.Z. Fiz. (1973) 154.

73M Mercurio, J. P., Etourneau, J., Naslain, R., Hagenmuller, P.: Mater. Res. Bull. 8 (1973) 837.

73S1 Sperlich, G., Buschow, K. H. J.: Proc. 4th. Int. Conf Solid Comp. Trans. Elements, Geneva, 1973, p. 216.

73S2 Sperlich, G.: Int. J. Magn. 5 (1973) 125.

73S3 Samsonov, G.V., Paderno, Yu.B., Levandovski, B.D., Konovalova, E.S.: in: Redkosemelnie metalli splabi i coedinenia, Isdatelstvo NAUKA ed., Moscow, 1973, p. 269 (in Russian).

75A Andres, K., Graebner, J. E., Ott, H. R.: Phys. Rev. Lett. 35 (1975) 1779.

75G1 Glaunsinger, W. S.: Phys. Status Solidi (b) 70 (1975) K 151.

75G2 Glaunsinger, W. S.: J. Magn. Reson. 18 (1975) 265.

75S Samsonov, G. V., Serebryakova, T. I., Neronov, V. A.: Boridy, Moskva Atomizdat, 1975.

76A Amberger, E., Polborn, K.: Acta Crystallogr. B 32 (1976) 981.

76G1 Glaunsinger, W. S.: AIP Conf. Proc. 1976 (Magn. Mat. Ann. Conf. 21th, 1975) 412.

76G2 Glaunsinger, W. S.: Phys. Status Solidi (b) 74 (1976) 443.

76G3 Glaunsinger, W. S.: J. Phys. Chem. Solids 37 (1976) 51.

76G4 Glaunsinger, W. S.: J. Magn. Reson. 21 (1976) 147.

76T Tanaka, T., Akahane, T., Bannai, E.: J. Phys. C 9 (1976) 1235.

77B1 Berezin, A. A., Golikova, O. A., Zaitsev, V. R., Kazanin, M. M., Orlov, V. M., Tkalenko, E. N., in:Boron and Refractory Borides, (Matkovich V. 1., ed.) Springer: Berlin, Heidelberg, New York 1977, p. 52.

77B2 Busehow, K. H. J.: see [77B1], p. 494.

77E Etourneau, J., Mercuno, J. P., Hagenmuler, P.: see [77B1], p. 115.

77K Kasuya, T., Kojima, K., Kasaya, M.: see [77A], p. 137.

77O Oudet, X.: see [77B1], p. 525.

77T Tanaka, T., Yoshimoto, J., Ishii, M.: Solid State Commun. 22 (1977) 203.

78A Allen, J. W., Martin, R. M., Batlogg, B., Wachter, P.: J. Appl. Phys. 49 (1978) 2078.

78R Report Nat. Inst. Research in Inorg. Mater. 17 (1978) 44.

79A Allen, J. W., Batlogg, B., Wachter, P.: Phys. Rev. 20B (1979) 4807.

79G Gurin, V. N., Korsukova, M. M., Nikanorov, S. P., Smirnov, I. A., Stepanov, N. N., Shulman, S. G.: J. Less-Common Met. 67 (1979) 115.

79K Kunii, S., Kasuya, T.: J. Phys. Soc. Jpn. 46 (1979) 13.

79M Mercuno, J. P., Angelov, S., Etourneau, J.: J. Less-Common Met. 67 (1979) 237.

79M2 Martin, R. M., Allen, J. W.: J. Appl. Phys. 50 (1979) 7561.

79O Oseroff, S., Calvo, R., Stankiewicz, J., Fisk, Z., Johnston, D. C.: Phys. Status Solidi (b) 94 (1979) K 133.

79P Paderno, Yu.B., Konovalova, E.S.: J. Less-Common Met. 67 (1979) 185.

79S Swanson, LW., Mc Neely, D. R.: Surf. Sci. 83 (1979) 11.

79T Tsai, C.C.: Phys. Rev. B 19 (1979) 2041.

80F Futamoto, M., Nakazawa, M., Kawabe, U.: Surf. Sci. 100 (1980) 470.

80H Holtzberg, F., v. Molnar, S., Coly, J. M. D.: Handbook on Semicond., Vol. 3 (ed. Keller, S. P.) North Holland: Amsterdam, 1980, p. 803.

80L Lannin, J.S., Messier, R.: Phys. Rev. Lett. 45 (1980) 1119.

81F Finkel'shtein, L.D., Efremova, N.N., Konovalova, E.S., Paderno, Yu.B.: Fiz. Tverd. Tela 23 (1981) 3465 (in Russian).

81K Korsukova, M.M., Stepanov, N.N., Gontcharova, E.V., Gurin, V.N., Nikanorov, S.P., Smirnov, I.A.: J. Less-Common Met. 82 (1981) 211. (Proc. 7th Int. Symp. Boron, Borides and Rel. Compounds, Uppsala, Sweden, 1981).
81M Moiseenko, L.L., Avtoref, L.L.: Thesis, Kiev, 1981, p. 24.
81P Pena, O., MacLaughlin, D. E., Lysak, M.: J. Appl. Phys. 52 (1981) 2152.
81S Shelykh, A.I., Sidorin, K.K., Karin, M.G., Bobrikov, V.N., Korsukova, M.M., Gurin, V.N., Smirnov, I.A.: J. Less-Common Met. 82 (1981) 291.
81T Takigawa, M., Yasuoka, H., Kitaoka, Y., Tanaka, T., Nozaki, H., Ishizawa, Y.: J. Phys. Soc. Jpn. 50 (1981) 2525.
82A Aita, O., Watanabe, T., Fujimoto, Y., Tsutsumi, K.: J. Phys. Soc. Jpn. 51 (1982) 483.
82F Flachbart, K., Rieffers, M., Janos, S., Paderno, Yu.B., Lazorenko, V.I., Konovalova, E.S.: J. Less-Common Met. 88 (1982) L11.
82K Konovalova, E.S., Paderno, Yu.B., Lundstrem, T., Finkel´shtein, L.D., Efremova, N.N., Dudnik, E.M.: Sov. Powder Metall. Met. Ceram. 21 (1982) 820.
82O Okusawa, M., Ichikawa, K., Matsumoto, T., Tsutsumi, K.: J. Phys. Soc. Jpn. 51 (1982) 1921.
82T Tsutsumi, K., Aita, O., Watanabe, T.: Phys. Rev. 25B (1982) 5415.
83A1 Aliev, F.G., Brandt, N.B., Moshtshalkov, V.V., Pashkevich, S.N., Paderno, Yu.B., Konovalova, E.S., Gurin, V.N., Smirnov, I.A.: Fiz. Tverd. Tela 25 (1983) 2579 (in Russian).
83A2 Alvazov, M.I., Aleksandrovich, S.V., Avseev, B.A., Mkrtchyab, V.B., Tsarev, O.M.: Inorg. Mater. 19 (1983) 191.
83B Berman, I.V., Brandt, H.B., Moshtshalkov, V.V., Pashkevich, S.N., Sidorov, V.I., Konovalova, E.S., Paderno, Yu.B.: Mosk. Gos. Univ. im. M.V. Lomonosova 38 (1983) 393 (in Russian).
83F Farberovich, O.V., Kurganskii, S.I., Sidorin, K.K., Karin, M.G., Bobrikov, V.N., Nizhnikova, G.P., Shelikh, Korsukova, M.M., Gurin, V.N.: Sov. Phys. Solid State 25 (1983) 404 (Engl. Transl.); Fiz. Tverd. Tela 25 (1983) 708 (in Russian).
83K Kasuya, T., Kasaya, M., Takegahara, K., Fujita, T., Goto, T., Tamaki, A., Takigawa, M., Yasuoka, H.: J. Magn. Magn. Mater. 31-34 (1983) 368.
83P Paderno, Yu.B., Lundström, T.: Acta Chem. Scand. A 37 (1983) 609.
83T Takigawa, M., Yasuoka, H., Tanaka, T., Ishizawa, Y., Kasaya, M., Kasuya, T.: J. Magn. Magn. Mater. 31-34 (1983) 391.
84K Konovalova, E.S., Paderno, Yu.B., Perepeliza, N.I., Dudnik, E.M., Yanosh, Sh., Flachbart, K., Reiffers, M.: Fiz. Tverd. Tela 26 (1984) 2138 (in Russian).
84L Lundström, T.: J. Less-Common Met. 100 (1984) 215.
85P1 Peysson, Y., Ayache, C., Sales, B.: J. Magn. Magn. Mater. 47 & 48 (1985) 63.
85P2 Prosandeev, S.A., Soldatov, A.V., Paderno, Yu.B., Konovalova, E.S.: Sov. Phys. Solid State 27 (1985) 181.
85S1 Schwetz, K.A., Lipp, A.: in: Ullmann's Encyclopedia of Industrial Chemistry, VCH: Weinheim, 1985, p. 295.
85S2 Smith, H.G., Dolling, G., Kunii, S., Kasaya, M., Liu, B., Takegahara, K., Kasuya, T., Goto, T.: Solid State Commun. 53 (1985) 15.
86B Borovikova, M.S., Fesenko, V.V.: J. Less-Common Met. 117 (1986) 287. (Proc. 8th Int. Symp. Boron, Borides, Carbides, Nitrides and Rel. Compounds, Tbilisi, Oct. 8 - 12, 1984)
86G Gruhl, H., Winzer, K.: Solid State Commun. 57 (1986) 67.

87A Abel'skii, Sh.Sh., Zilishikhis, A.L., Irkhin, U.P., Kryuk, V.I., Knyshev, E.A., Riabin, V.A.: in: Proc. 9th Int. Symp. Boron, Borides and Rel. Compounds, University of Duisburg, Germany, Sept. 21 - 25, 1987, H. Werheit ed., University of Duisburg: Duisburg, 1987, p. 377.

87K1 Korsukova, M.M., Lundström, T., Tergenius, L.E., Gurin, V.N.: Solid State Commun. 63 (1987) 187.

87K2 Korsukova, M.M., Lundström, T., Tergenius, L.-E., Gurin, V.N.: in: Proc. 9th Int. Symp. Boron, Borides and Rel. Compounds, University of Duisburg, Germany, Sept. 21 - 25, 1987, H. Werheit ed., University of Duisburg: Duisburg, 1987, p. 334.

87P Paderno, Yu.B., Konovalova, E.S.: in: Proc. 9th Int. Symp. Boron, Borides and Rel. Compounds, University of Duisburg, Germany, Sept. 21 - 25, 1987, H. Werheit ed., University of Duisburg: Duisburg, 1987, p. 65.

87W Wachter, P.: in: Proc. 9th Int. Symp. Boron, Borides and Rel. Compounds, University of Duisburg, Germany, Sept. 21 - 25, 1987, H. Werheit ed., University of Duisburg: Duisburg, 1987, p. 166.

88A Alekseev, P.A., Konovalova, E.S., Lasukov, V.N., Lyukshina, S.I., Paderno, Yu.B., Sadikov, I.P., Udovenko, E.V.: Fiz. Tverd. Tela 30 (1988) 2024 (in Russian).

89S Sidorov, V.A., Stepanov, N.N., Ziok, O.B., Cheostanzev, L.G., Smirnov, I.A., Korsukova, M.M.: Fiz. Tverd. Tela 31 (1989) 197 (in Russian).

90K1 Konovalova, E.S., Paderno, Yu.B., Lyukshina, S.I., Yuchimenko, E.V.: Neorg. Mater. 26 (1990) 1218.

90K2 Konovalova, E.S., Paderno, Yu.B., Filippov, V.B., Efremova, N.N., Flachbart, K., Bat'ko, I., Kavezanski, B., Gudak, O.: Neorg. Mater. 26 (1990) 1432.

91A Alekseev, P.A., Ivanov, A.S., Kikoin, K.A., Mischenko, A.S., Lazukov, A.N., Rumyantsev, A.Yu., Sadikov, I.P., Konovalova, E.S., Paderno, Yu.B.: in: Boron-Rich Solids, Proc. 10th Int. Symp. Boron, Borides and Rel. Compounds, Albuquerque, NM 1990 (AIP Conf. Proc. 231), D. Emin, T.L. Aselage, A.C. Switendick, B. Morosin, C.L. Beckel ed., American Institute of Physics: New York, 1991, p. 318.

91S1 Sidorov, V.A., Stepanov, N.N., Ziok, O.B., Chvostanzev, L.G., Smirnov, N.A., Korsukova, M.M.: Fiz. Tverd. Tela 33 (1991) 1271(in Russian).

91S2 Shitsevalova, N.Yu., Paderno, Yu.B.: in: Boron-Rich Solids, Proc. 10th Int. Symp. Boron, Borides and Rel. Compounds, Albuquerque, NM 1990 (AIP Conf. Proc. 231), D. Emin, T.L. Aselage, A.C. Switendick, B. Morosin, C.L. Beckel ed., American Institute of Physics: New York, 1991, p. 326.

91T Trounov, V.A., Malyshev, A.L., Chernyshov, D.Yu., Korsukova, M.M., Gurin, V.N., Aslanov, L.A., Chernyshev, V.V: J. Appl. Crystallogr. 24 (1991) 888.

93A1 Alekseev, P.A.: Physica B 186-188 (1993) 365.

93A2 Aselage, T.L., Emin, D., Samara, G.A., Tallant, D.R., van Deusen, S.B., Eatough, M.O., Tardy, H.L., Venturini, E.L.: Phys. Rev. B 48 (1993) 11759.

93A3 P.A. Alekseev, J.M. Mignod, J. Rossad-Mignod, V.N. Lazukov, I.P. Sadikov, Physica B 186/188, 384 (1993).

93T Trounov, V.A., Malyshec, A.L., Chernyshov, D.Yu., Korsukonva, M.M., Gurin, V.N., Aslanov, L.A., Chernychev, V.V.: J. Phys.: Condens. Matter 5 (1993) 2479.

94C Chernyshev, D. Yu., Korsukova, M.M., Malyshev, A.L., Gurin, V.N., Trunov, V.A., Chernyshev, V.V., Aslanov, L.A.: Phys. Solid State 36 (1994) 585.

94G Gurin, V.: Proc. 11th Int. Symp. Boron, Borides and Rel. Compounds, Tsukuba, Japan, August 22 - 26, 1993, Jpn. J. Appl. Phys. Series 10 (1994), p. 138.

94K1 Konovalova, E., Paderno, Yu.B., Khoynenko, N.: Proc. 11th Int. Symp. Boron, Borides and Rel. Compounds, Tsukuba, Japan, August 22 - 26, 1993, Jpn. J. Appl. Phys. Series 10 (1994), p. 126.

94K2 Korsukova, M.M.: Proc. 11th Int. Symp. Boron, Borides and Rel. Compounds, Tsukuba, Japan, August 22 - 26, 1993, Jpn. J. Appl. Phys. Series 10 (1994), p. 15.

94T Trunov, V.A., Malyshev, A.L., Chernyshev, D.Yu., Korsukova, M.M., Gurin, V.N.: Phys. Solid State 36 (1994) 1465.

95A Alekseev, P.A., Mignod, J.M., Rossat-Mignod, J., Lazukov, V.N., Sadikov, I.P., Kanovalova, E.S., Paderno, Yu.B.: J. Phys.: Condens. Matter 7 (1995) 289.

96G Gurin, V.N., Derkachenko, L.I., Korsukova, M.M., Nikanorov, S.P., Jung, W., Müller, R.: Sov. Phys. Solid State 38 (1996) 1508.

97A Alekseev, P.A., Mignot, J.M., Lazukov, V.N., Sadikov, I.P., Paderno, Yu.B., Konovalova, E.S.: J. Solid State Chem. 133 (1997) 230 (Proc. 12th Int. Symp. Boron, Borides and Rel. Compounds, Baden, Austria, 1996).

97S Schmechel, R., Werheit, H., Paderno, Yu.B.: J. Solid State Chem. 133 (1997) 264 (Proc. 12th Int. Symp. Boron, Borides and Rel. Compounds, Baden, Austria, 1996).

98A Ambler, B., Fisk, Z., Sarrao, J.L., v. Molnar, S., Meisel, M.W., Sharifi, F.: Phys. Rev. B 57 (1998) 8747.

99D Dressel, M., Gorshunov, B.P., Sluchanko, N.E., Volkov, A.A., Hendersen, B., Grüner, G., Knebel, G., Loidl, A., Kunii, S.: Phys. Status Solidi (b) 215 (1999) 161.

99G Gorshunov, B., Sluchanko, N., Volkov, A., Dressel, M., Knebel, G., Loidl, A., Kunii, S.: Phys. Rev . B 59 (1999) 1808.

99O Otani, S., Nakagawa, H., Nishi, Y., Kieda, N.: J. Solid State Chem. (2000) (Proc. 13th Int. Symp. Boron, Borides and Rel. Compounds, Dinard, France, Sept. 1999).

99T Takahashi, Y., Ohshima, K., Okamura, F.P., Otani, S., Tanaka, T.: J. Phys. Soc. Jpn. 68 (1999) 2304.

99W Werheit, H., Au, T., Schmechel, R., Paderno, Yu.B., Konovalova, E.S.: J. Solid State Chem. (2000) (Proc. 13th Int. Symp. Boron, Borides and Rel. Compounds, Dinard, France, Sept. 1999).

Fig. 1.

SmB_6. NMR determined nuclear relaxation rate in samples prepared by different methods: *(1)* arc melting ($\rho(T < 4K) = 1 \cdot 10^{-2}\Omega$cm), *(2)* floating zone (single crystal, $\rho(T < 4K) = 70\ \Omega$cm), *(3)* floating zone (powder obtained by crushing a single crystal), *(4)* sintered, *(5)* Al-flux ($\rho(T < 4K) = 1...10\ \Omega$cm) [83T].

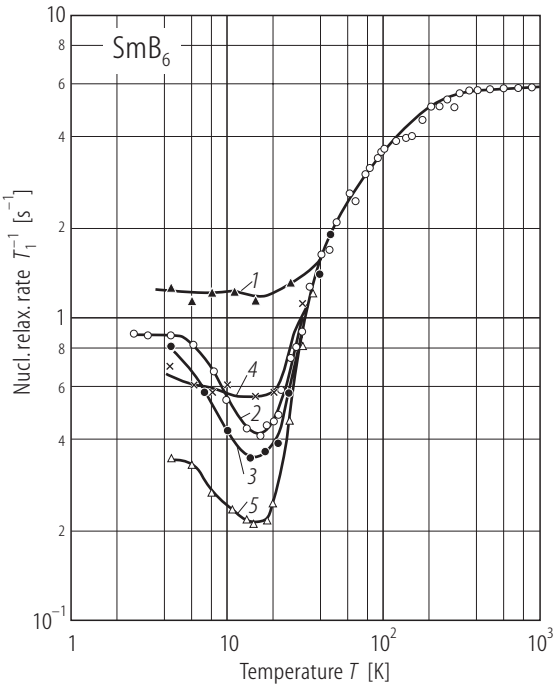

Fig. 2.

SmB_6. Calculated electronic band structure [83F].

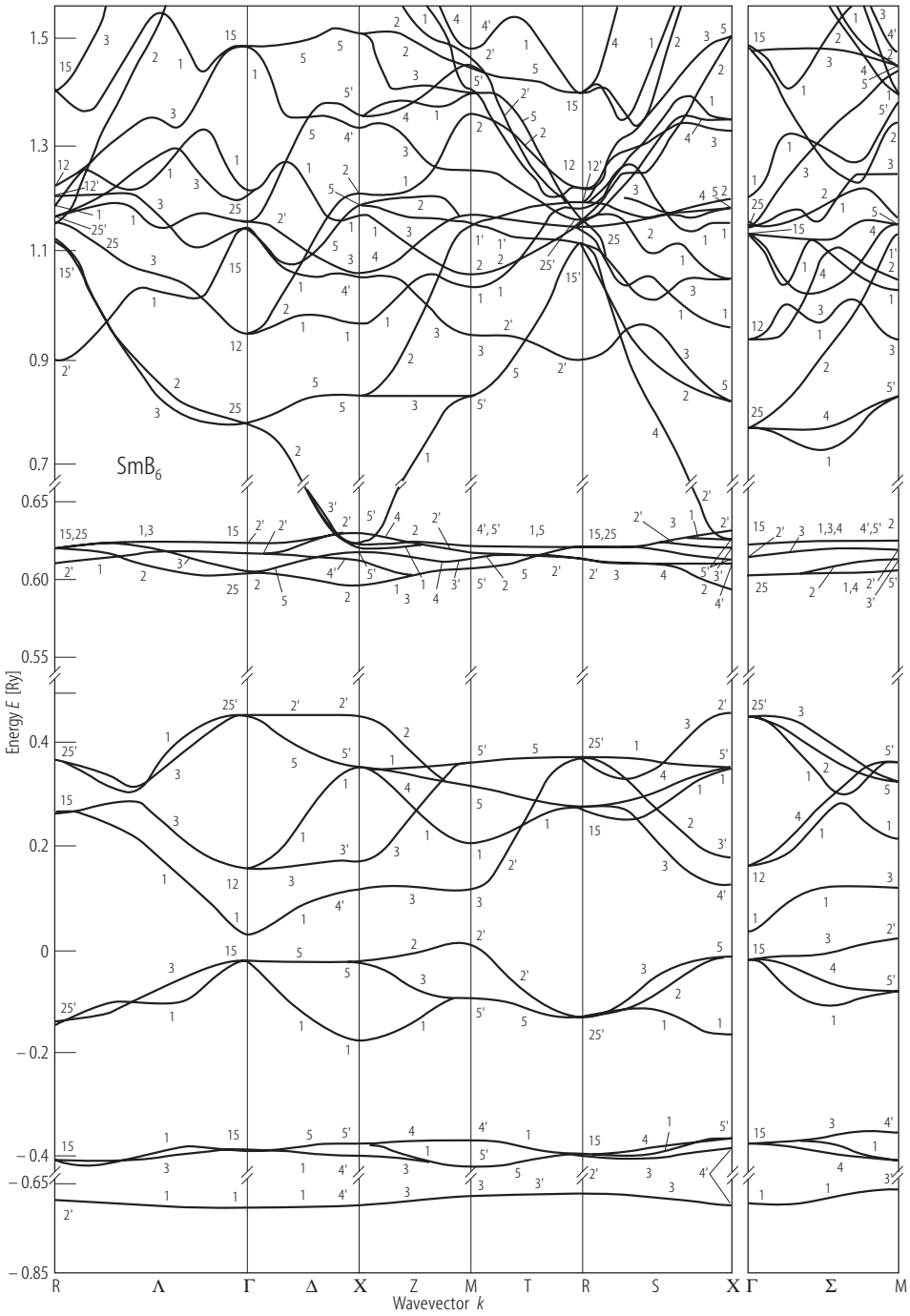

Fig. 3.

SmB_6. Energy band scheme derived from dc electrical conductivity and dynamical conductivity [99D, 99G].

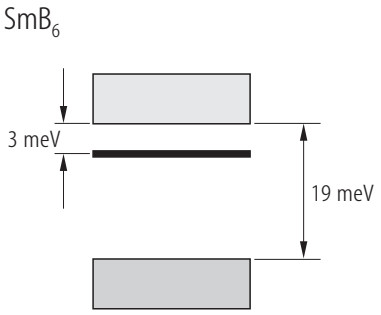

Fig. 4.

SmB_6. Frequency dependence of **(a)** conductivity and **(b)** dielectric constant. The (large) open circles correspond to the submm data; the open squares to the data at 35GHz; the arrow to the dc conductivity. The solid lines were obtained by the Kramers-Kronig analysis of the FIR reflectivity spectrum, combined with the spectra taken from [99G], [99D] and normalized at lowest frequencies to the reflectivity calculated from submm ε and σ. The large error bars for the IR conductivity correspond to a ± 0.25% uncertainty of the 3K reflectivity as obtained by the Kramers-Kronig analysis. The dashed lines are results of least-square fits. The shaded area correspond to the energy gap value of 19(2) meV. Insert in **(a)**, temperature dependence of the squared plasma frequency with two types of activated behavior: *(1)* 19 meV; *(2)* 3 meV. For a more detailed display of the low temperature data, see [99G].

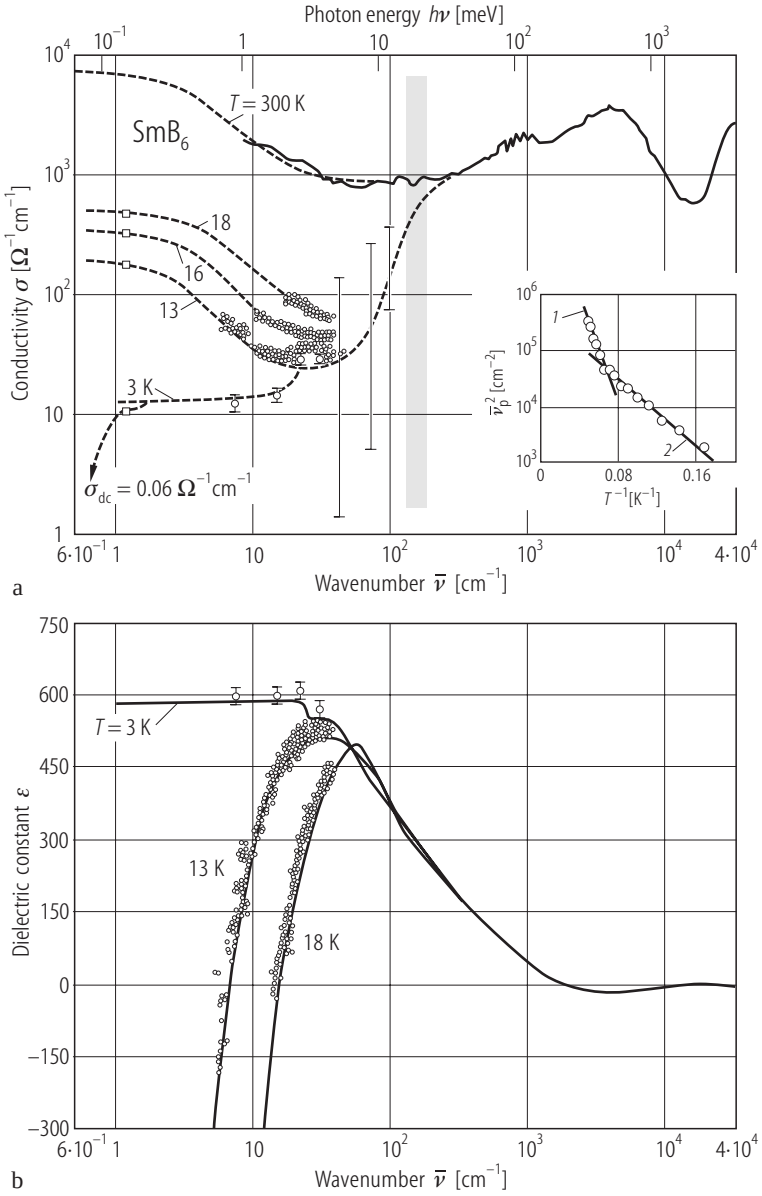

Fig. 5.

SmB_6. **(a)** Temperature dependencies of the plasma frequency ν_p of free charge carriers, of the scattering rate γ, and of the conductivity σ_{min} obtained by a model fit. Solid line (*1*), thermally activated (E_g = 19 meV); solid line *(2)*, thermally activated (E_d = 3 meV). **(b)** Temperature dependence of an oscillator in the submm range. ν_0, eigenfrequency, $\Delta\varepsilon$, dielectric contribution, γ, damping constant [99G].

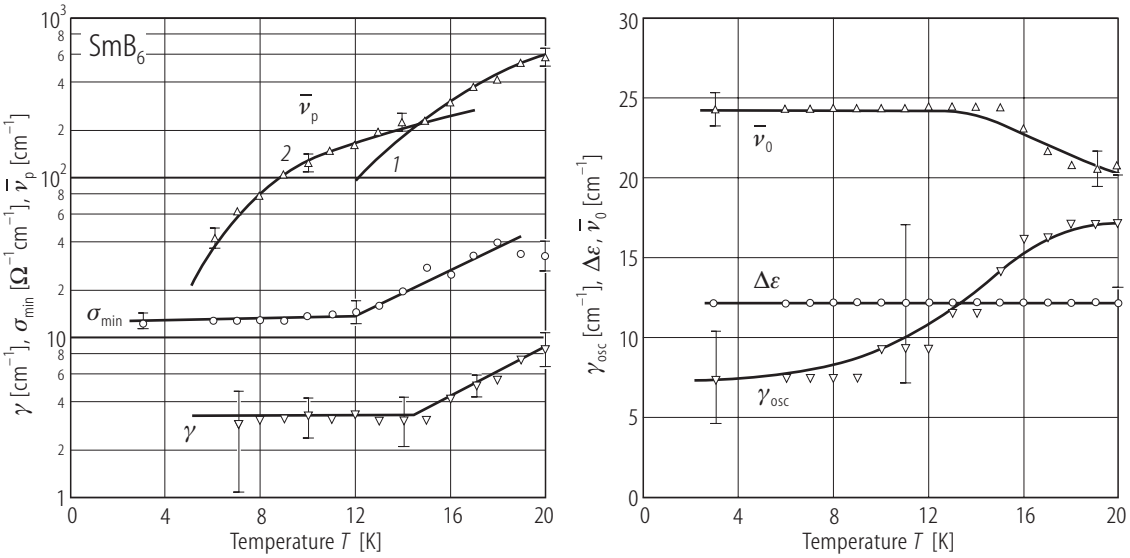

Fig. 6.

SmB_6. Electrical conductivity vs. reciprocal temperature [77E]; see also [77B2].

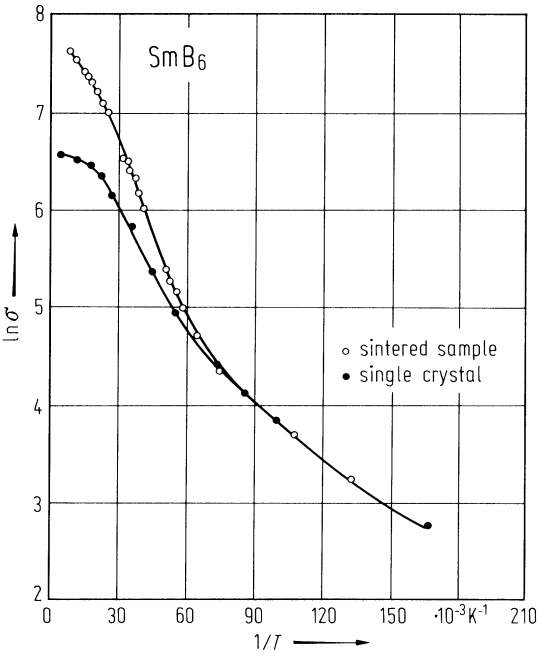

Fig. 7.

SmB_6. Pressure dependence of the energy gap derived from electrical conductivity; insert: assumed density of states distribution in the vicinity of the Fermi energy [83B].

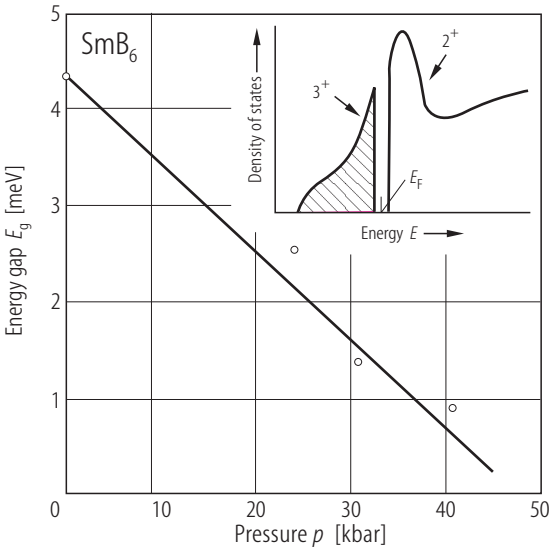

Fig. 8.

SmB_6. Interband density of states at 4 K calculated with the use of the resulting fit oscillator strength in the constant matrix element approximation. The dotted line gives the uncertainty between the peak with f character and that one with d character [87W].

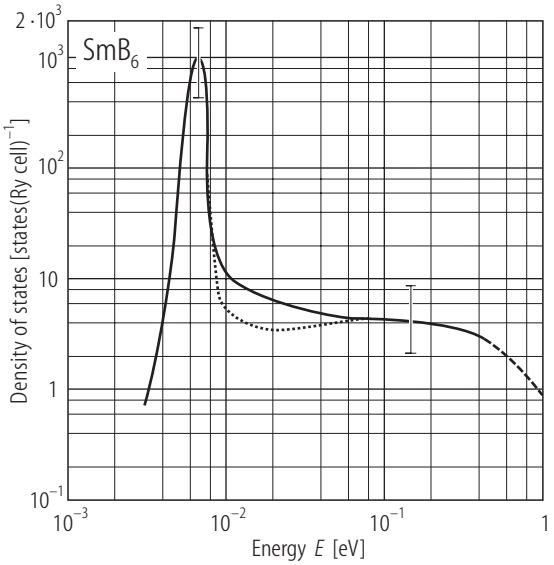

Fig. 9.

SmB_6 (:La, Eu, Gd). Lattice constants of $Sm_{1-x}La_xB_6$, $Sm_{1-x}Eu_xB_6$, $Sm_{1-x}Gd_xB_6$, vs. degree of substitution x [87P].

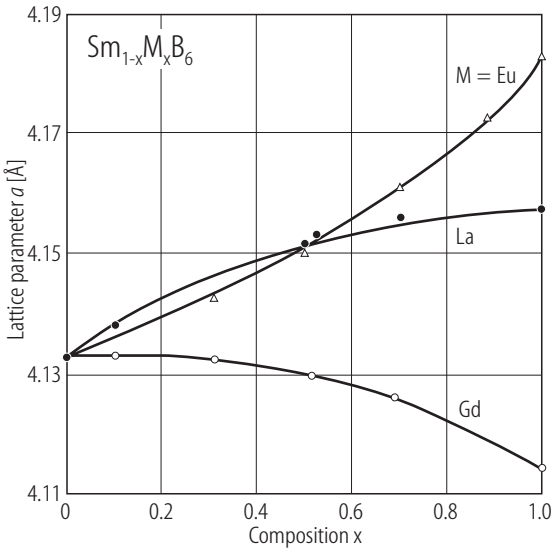

Fig. 10.

SmB_6. Effective valence of the Sm atoms vs. content of Eu, La, Yb, Dy, Ba, Gd atoms substituting for Sm [81F, 87P]. Note: in figure full circle should be for M = Ca instead of Eu.

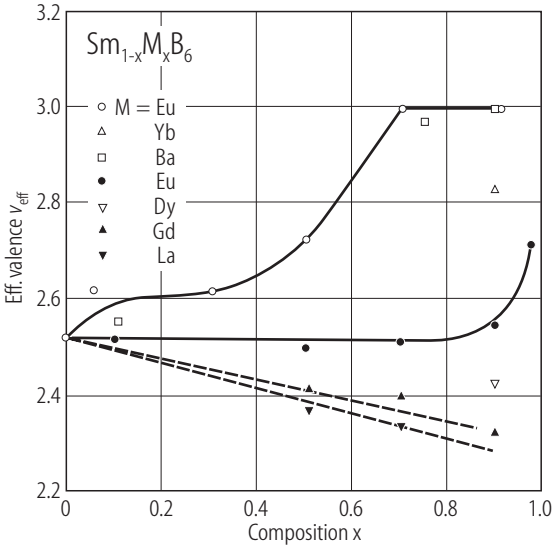

Fig. 11.

SmB_6 Effect of vacancies on the lattice parameter and on the valence state of Sm in Sm_xB_6 vs. x [82K].

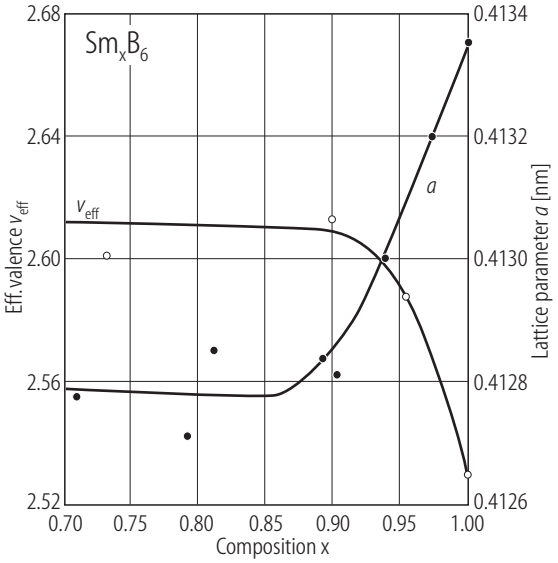

Fig. 12.

SmB_6. Temperature dependence of the electrical resistivity for SmB_6 with Ba, La, and Gd atoms substituted for Sm [84K].

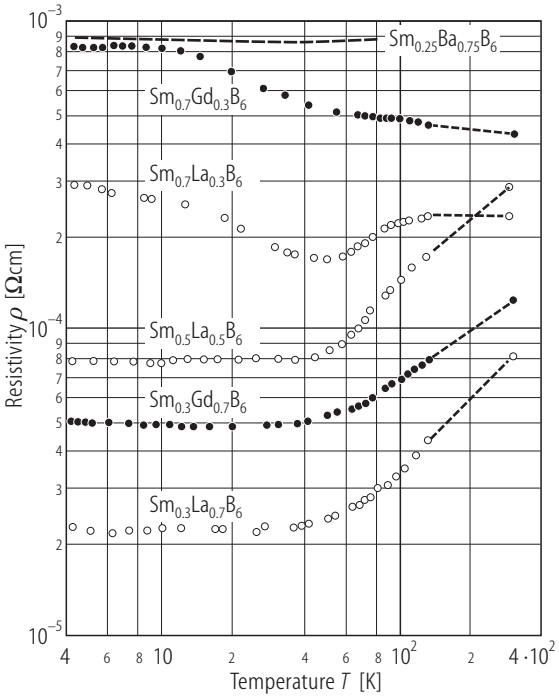

Fig. 13.

Metal hexaborides. Temperature dependence of the lattice parameters of CaB_6, $Sm_{0.05}Ca_{0.95}B_6$, $Sm_{0.4}Ca_{0.6}B_6$, SmB_6, $Sm_{0.5}La_{0.5}B_6$, LaB_6 determined by neutron scattering in [88A, 91A].

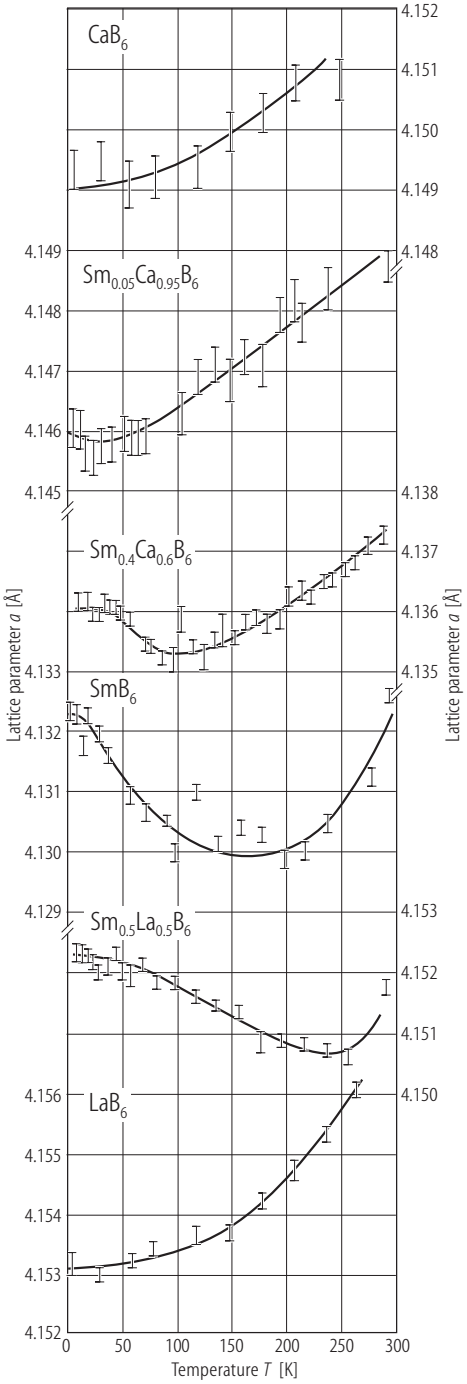

Fig. 14.

SmB_6. **(a)** Dependence of the electrical resistivity of $Sm_xLa_{1-x}B_6$ and $Sm_xGd_{1-x}B_6$ on the concentration of Sm atoms; **(b)** corresponding variation of the lattice parameters; T = 300 K [84K].

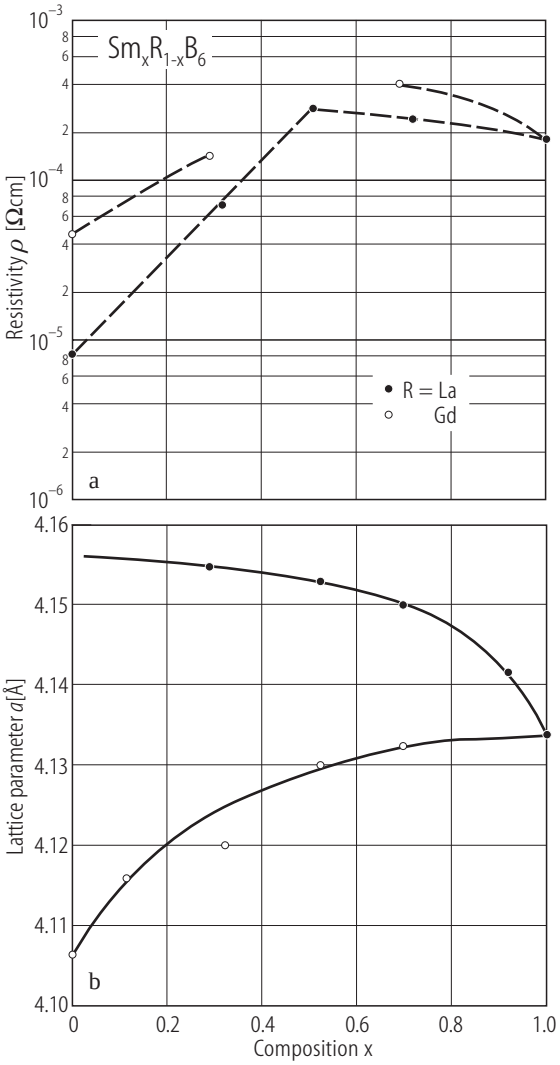

Fig. 15.

SmB_6. Thermal expansion $\Delta l/l$ vs. T; insert: derived linear thermal expansion coefficient [87W].

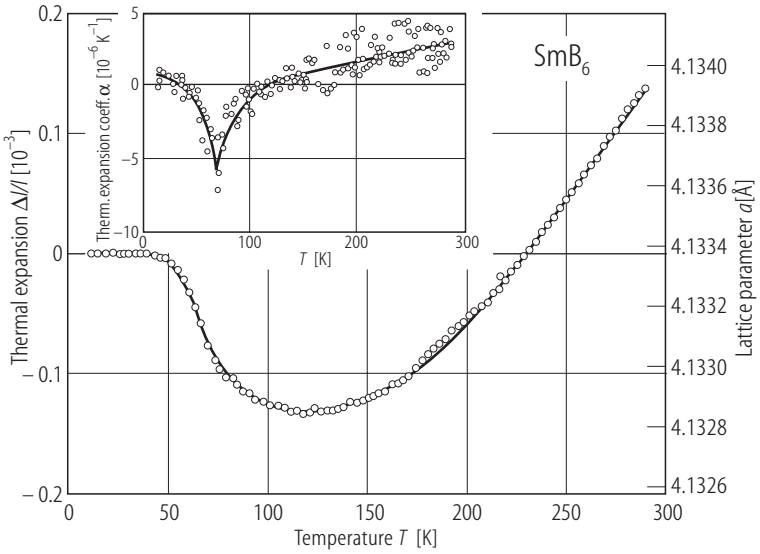

Fig. 16.

SmB_6. Lattice parameter a vs. T [93T].

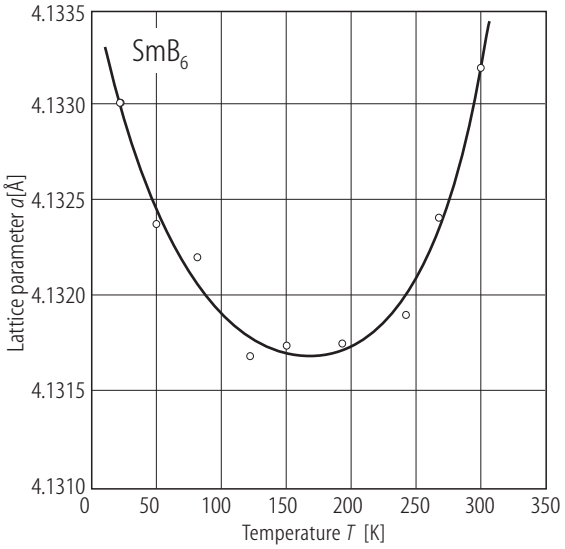

Fig. 17.

SmB_6. **(a)** Isotropic thermal parameter of the Sm atom; curve calculated in the Einstein model with Θ_E = 120 K; **(b)** anisotropic thermal parameters for the B atom in $^{154}Sm^{11}B_6$ [93T].

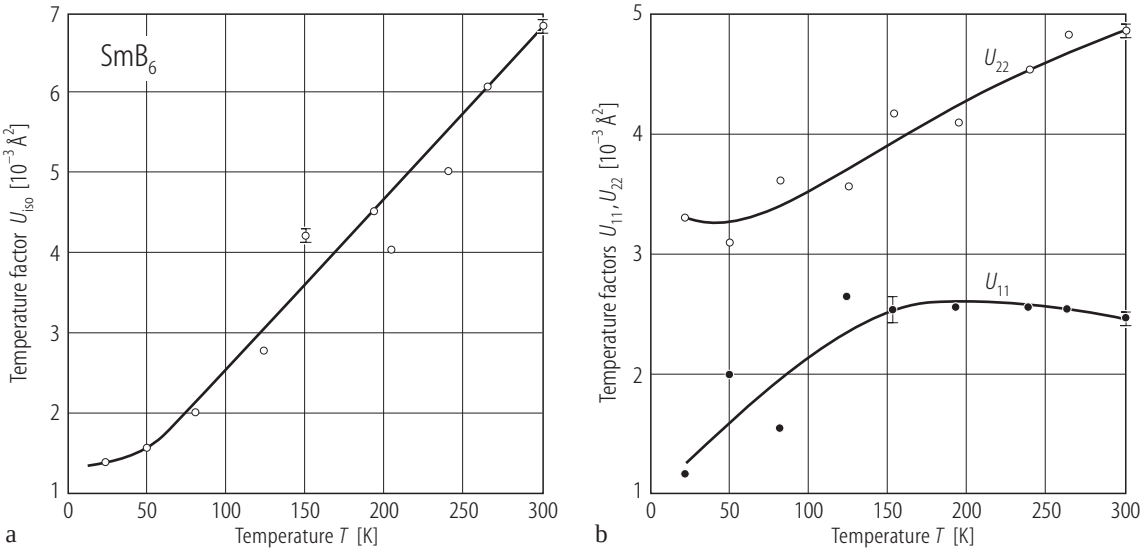

Fig. 18.

SmB_6. Effective Debye temperature vs. *T* [93T].

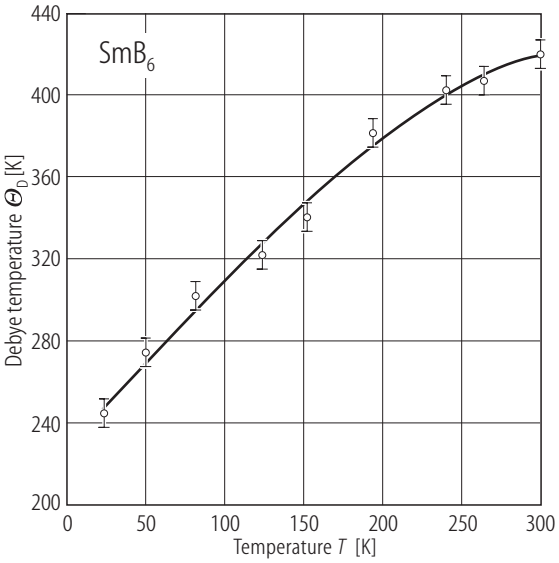

Fig. 19.

SmB_6. Phonon dispersion curves determined by inelastic neutron scattering. Points, experimental results; dashed lines, calculated dispersion curves for LaB_6 [91A].

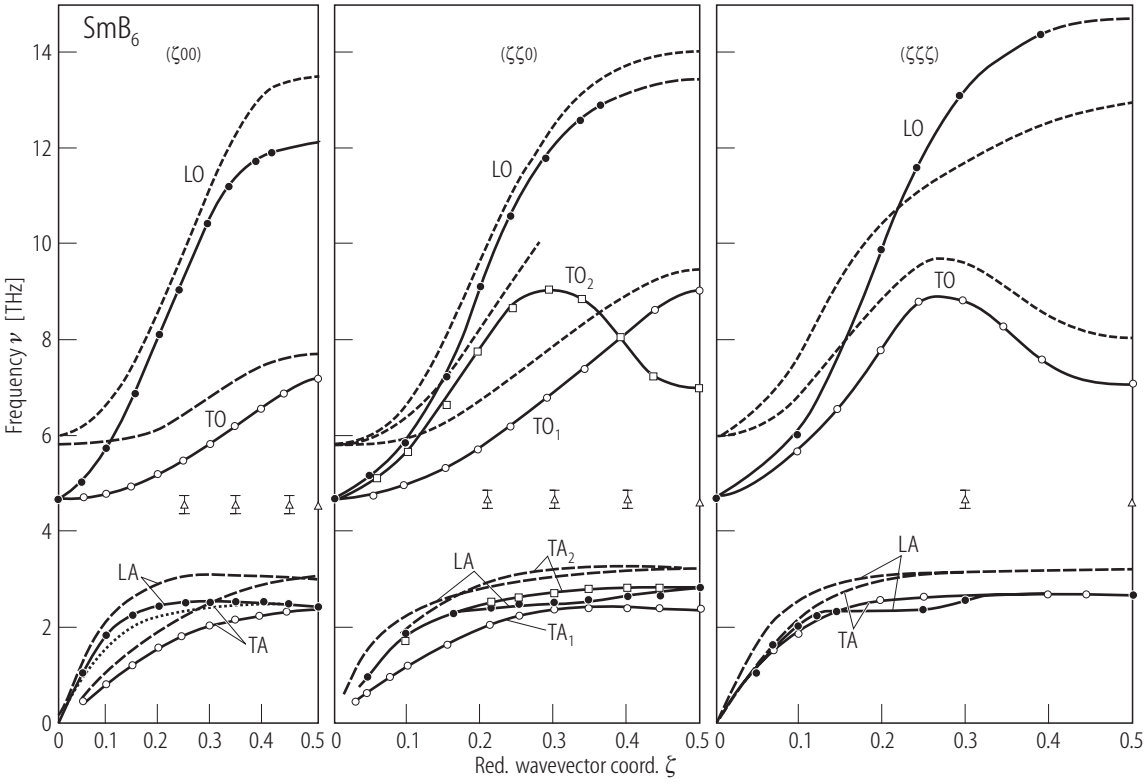

Fig. 20.

SmB_6. Low frequency part of the FT Raman spectrum [97S] and the FTIR spectrum [99W] compared with the phonon branches obtained on $^{154}Sm^{11}B_6$ by inelastic neutron scattering [91A, 93A2]. The considerable softening of the TO mode in the FT Raman spectrum compared with the spectra of neutron scattering and IR absorption is attributed to free carriers generated by the high intensity of the Nd:YAG laser (see [99W]).

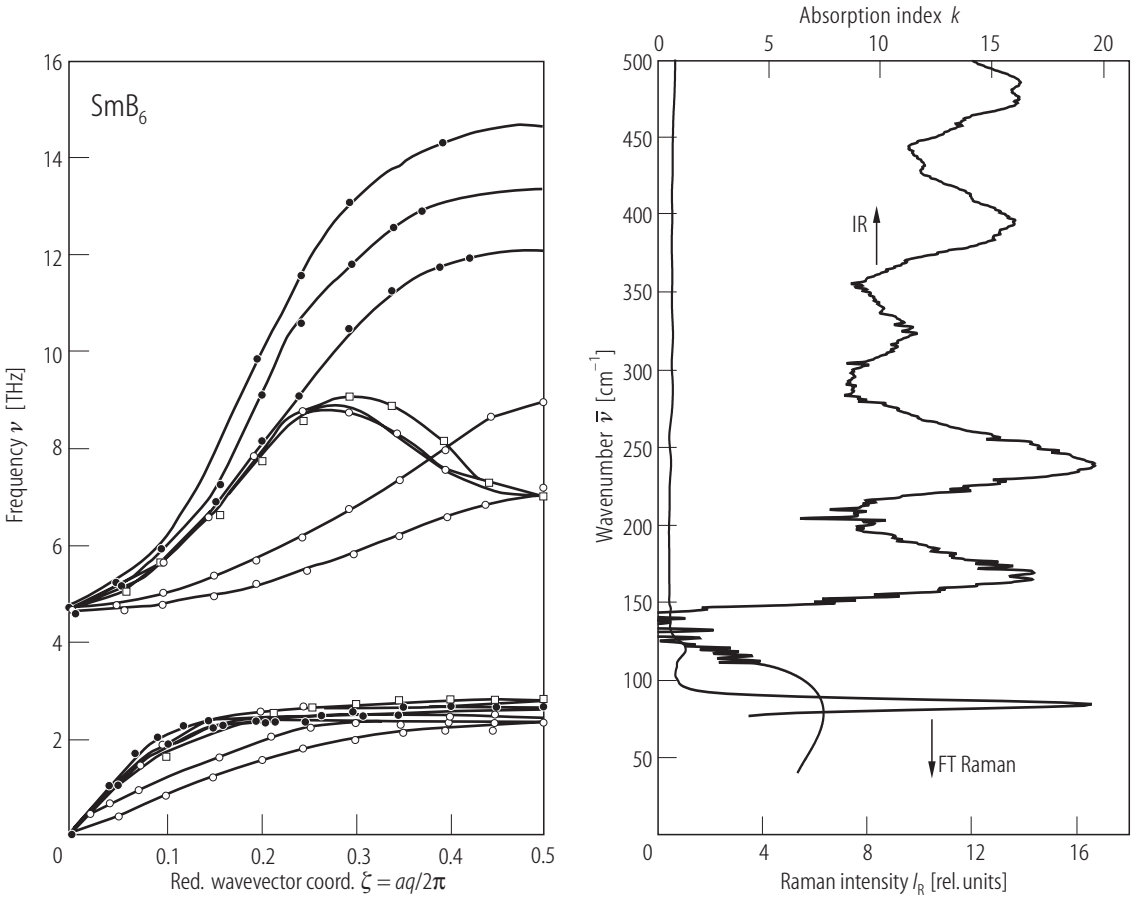

Fig. 21.

SmB_6. Phonon spectrum. Full lines, FT Raman spectrum (left ordinate) [97S]; dashed line, (right ordinate) conventionally measured Raman spectrum [81M], step-formed curve (right ordinate), inelastic neutron scattering [93A2].

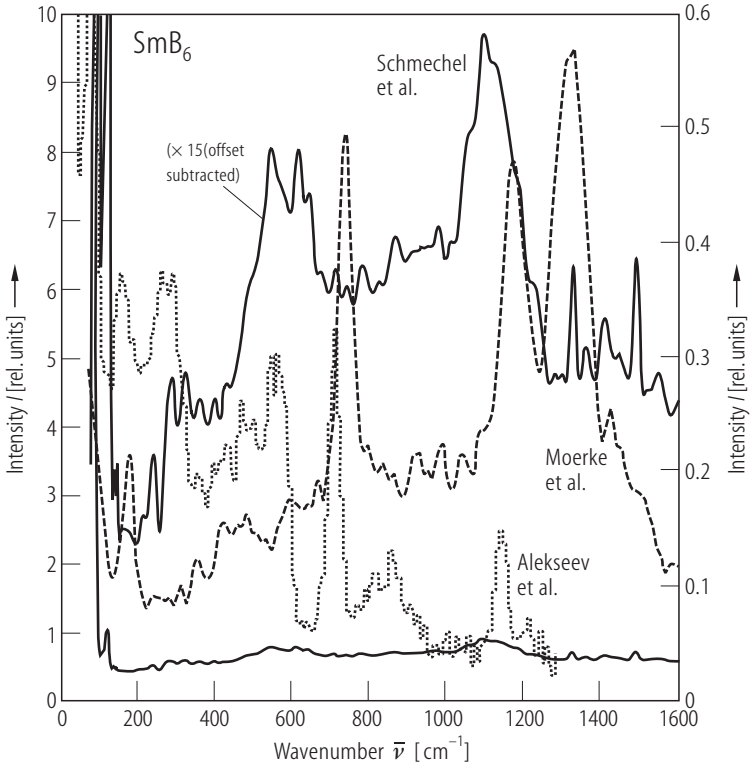

Fig. 22.

SmB_6. Electrical conductivity vs. reciprocal *T*. Full circles, small crystal [79A]; full triangles single crystal; dashed line, polycrystalline sample [82F, 84K]; full squares, single crystal (starting atomic ratio Sm:B = 1/7) prepared by the solution method [81K]. For Hall effect on the same samples see Fig. 30.

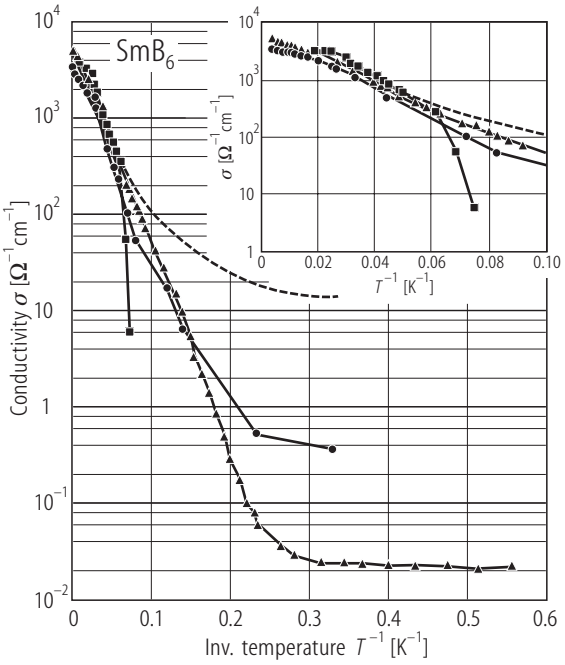

Fig. 23.

SmB_6. dc electrical conductivity, Arrhenius plot. Symbols, experimental results; line, $\sigma_{dc} \propto \exp[(3.5\ \text{meV})/k_B T]$; Fig. **(b)**, dc electrical conductivity in a double logarithmic scale; Fig. **(c)**, dc electrical conductivity vs $T^{-1/4}$ (Mott's law of variable-range hopping) [99G].

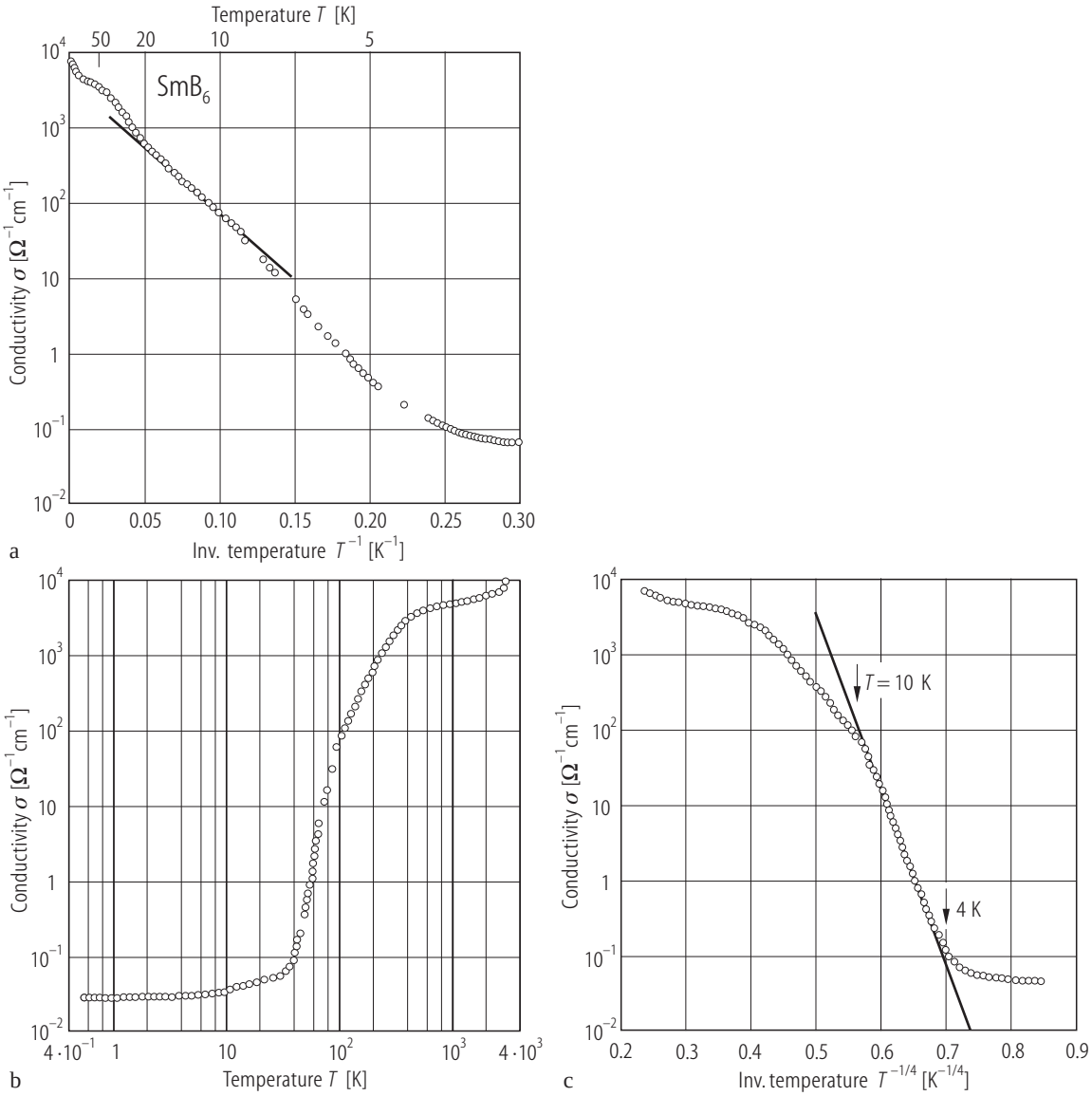

Fig. 24.

SmB_6. Temperature dependence of the resistance at different pressures: 0.2 kbar, 24 kbar, 40 kbar, 57 kbar, 70 kbar, 108 kbar [83B].

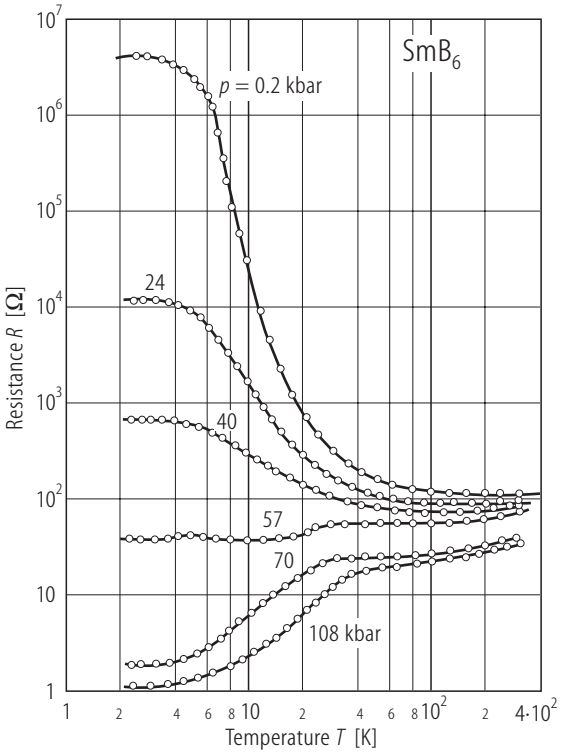

Fig. 25.

Metal hexaborides. Pressure dependence of the electrical resistivity; $\rho(p)/\rho(0)$ vs. hydrostatic pressure p. Full lines, monocrystalline LaB_6, EuB_6 and YbB_6 [91S1], dashed lines, LaB_6, SmB_6 prepared from starting ratios Sm:B 1/7, 1/9, 1/12 (effect increases this way), YbB_6, EuB_6 [81K].

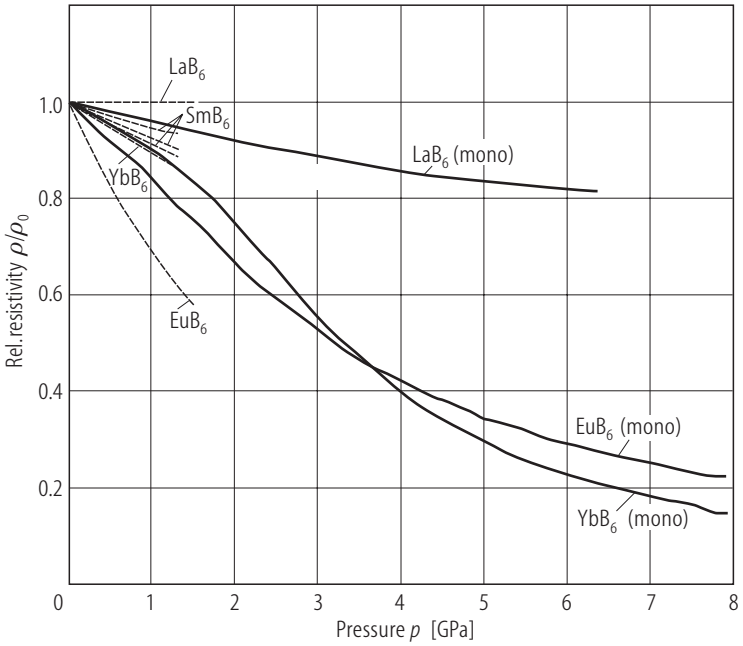

Fig. 26.

SmB_6. Resistivity and Hall mobility of SmB_6 samples vs. temperature [71N2]. The calculated curves are discussed in the original paper.

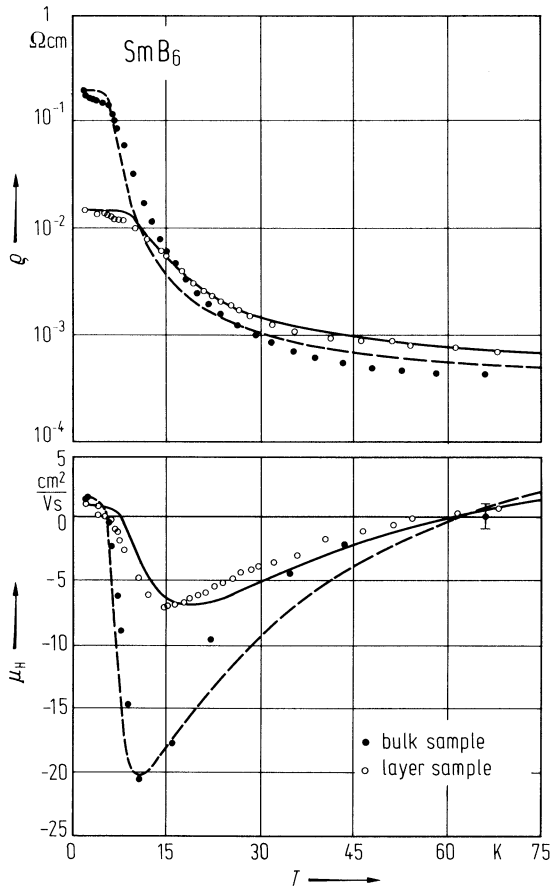

Fig. 27.

SmB_6. Temperature dependence of resistivity measured at 230 Hz; same samples as in Fig. 32 [79A].

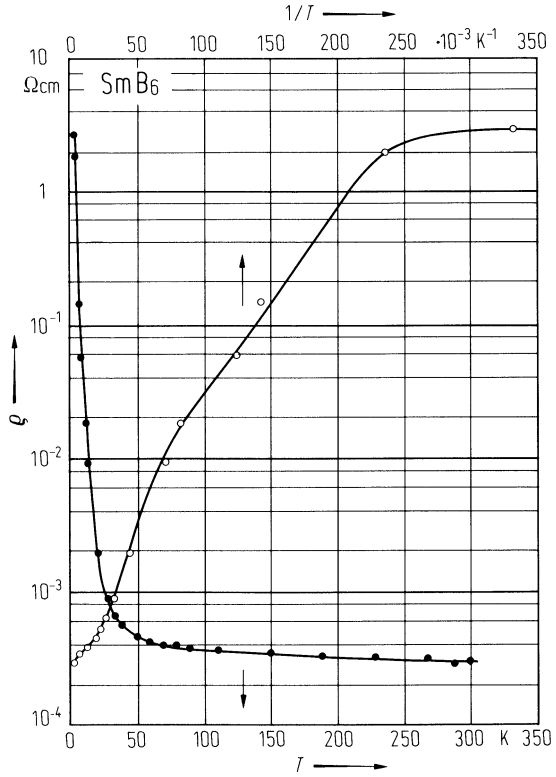

Fig. 28.

SmB_6. Thermoelectric power vs. temperature; data on two samples [69P, 73M, 77E].

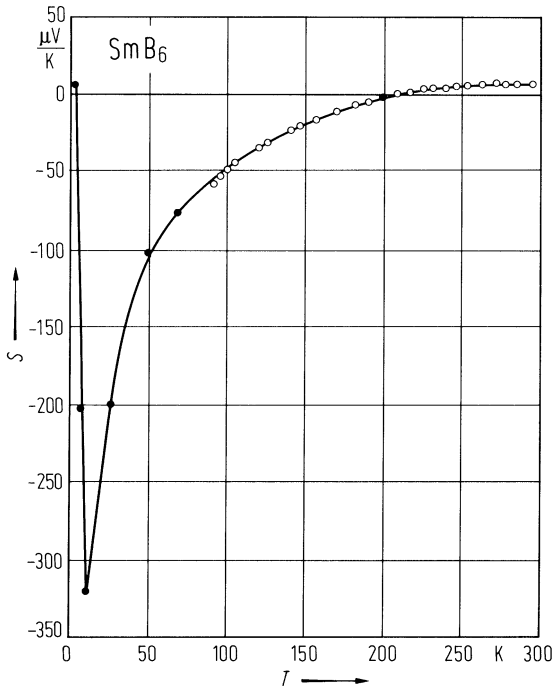

Fig. 29.

SmB_6. Pressure dependence of the thermoelectric power of monocrystals at 300 K; *S* vs. *p*. Curves (*1*), (*2*) and (*3*), *(4)* respectively for samples in different liquids [89S].

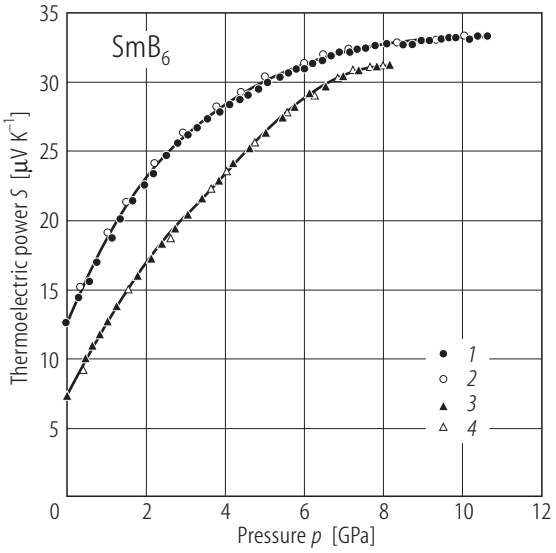

Fig. 30.

SmB_6. Temperature dependence of the Hall coefficient; R_H vs. reciprocal T. Full triangles: $R_H > 0$, open triangles: $R_H < 0$ [79A]; full circles: $R_H > 0$, open circles: $R_H < 0$ single crystals (starting atomic ratio Sm:B = 1/7) prepared by the solution method [81K]. For electrical conductivity of the same material, see Fig. 23.

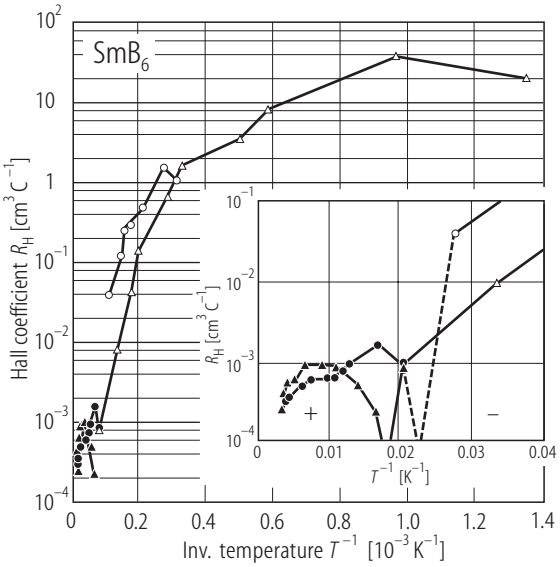

Fig. 31.

SmB_6. Magnetoresistance ; $\Delta\rho/\rho_0$ vs. B at T = 1.56 K and T = 4.2 K [84K, 83A1].

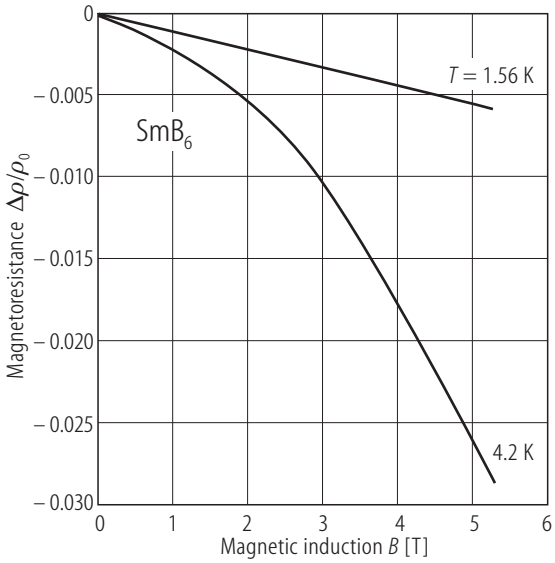

Fig. 32.

SmB_6. Temperature dependence of the Hall coefficient, measured at 230 Hz with B = 1.7 T: same samples as in Fig. 27 [79A].

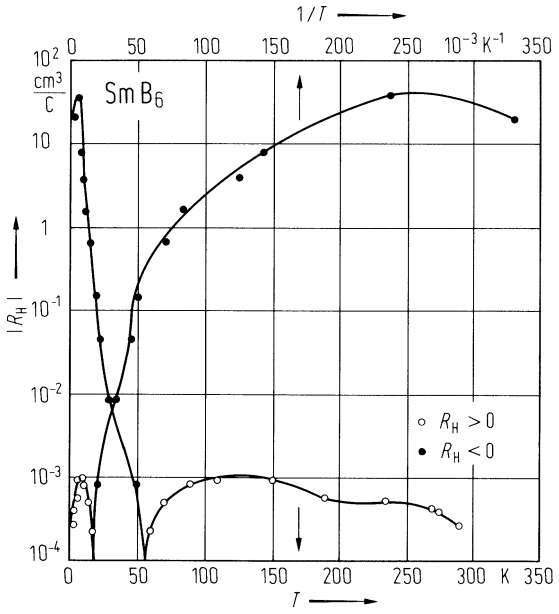

Fig. 33.

SmB_6. Real part of the optical conductivity vs. photon energy for 4 and 300 K. Fit for the low temperature curve with two oscillators (at 0.0055 and 0.1 eV with oscillator strengths of 0.00033 and 0.3 respectively) [87W].

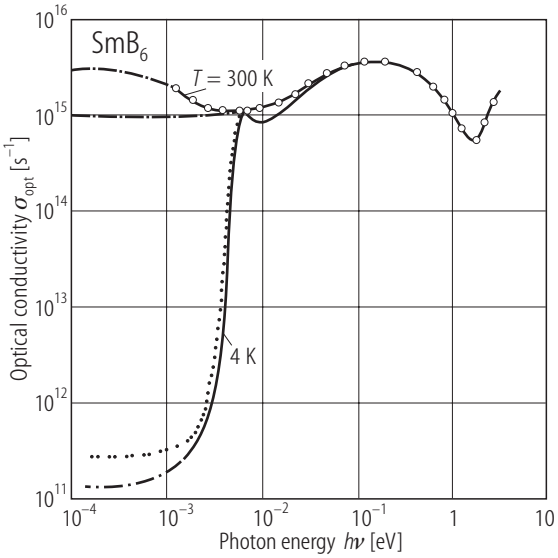

Fig. 34.

Metal hexaborides. Optical reflectivity spectra; R vs. photon energy. Long-dashed curve, LaB_6, solid curve, SmB_6, short-dashed curve, EuB_6 [81S].

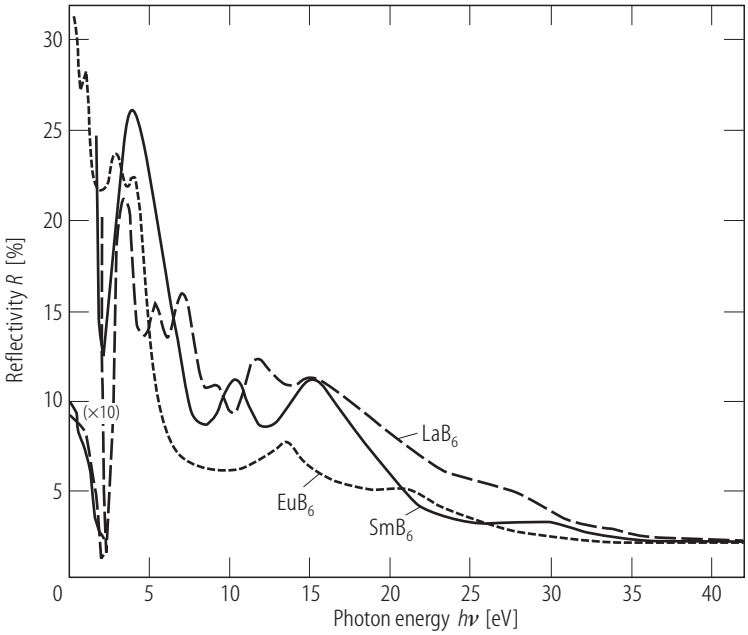

Fig. 35.

SmB_6. Dielectric function vs. photon energy. ε_1, real part, ε_2 imaginary part, –Im (ε^{-1}) energy loss function, ε^e contribution of free electrons (determined by making model assumptions for the interband transitions) [81S].

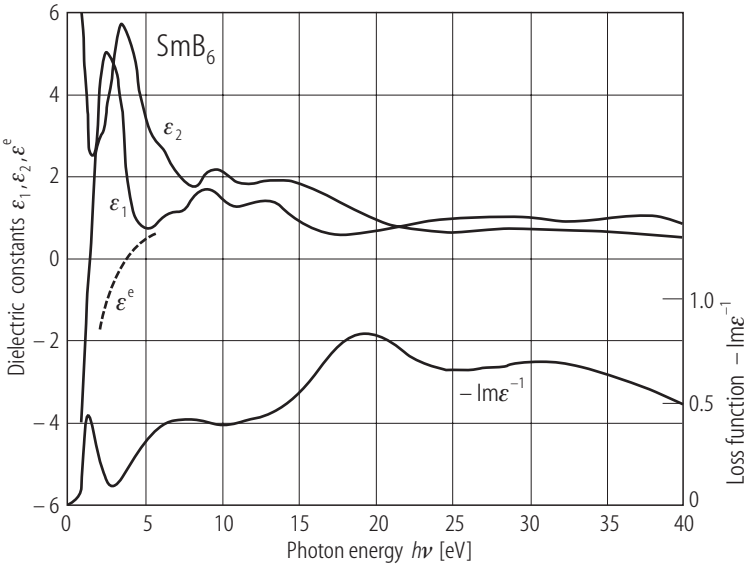

Fig. 36.

SmB_6. FIR reflectivity spectrum, R vs. photon energy, for 4 and 300 K [87W].

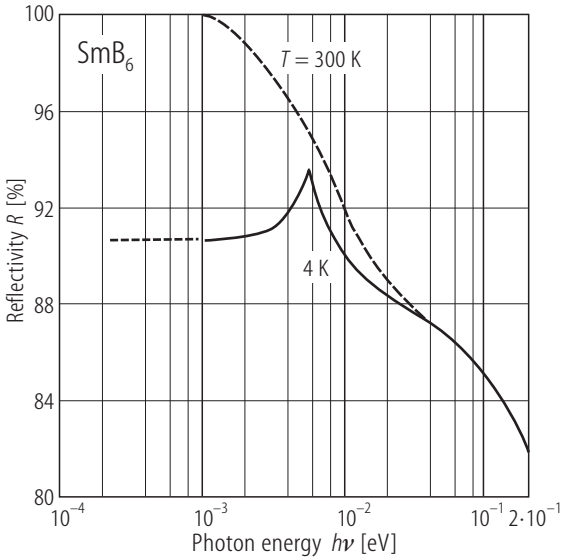

Fig. 37.

SmB_6. Magnetic susceptibility (in CGS-emu). The fit is based on the activation energy 6 meV, which corresponds to the separation of the two DOS peaks, which is 5.5 meV, while the gap energy is 4 meV [87W].

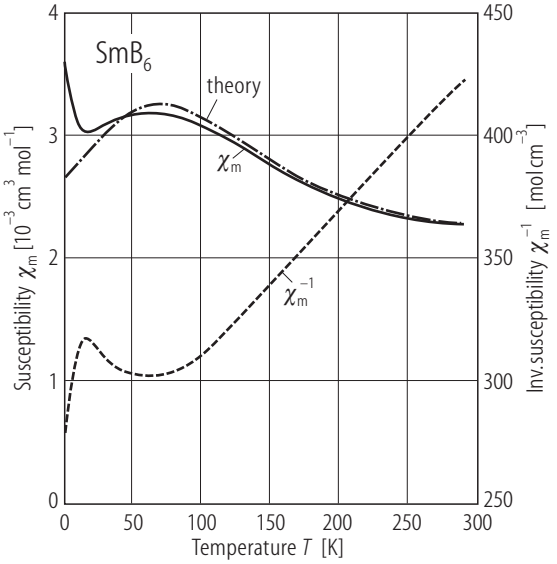

Fig. 38.

SmB_6. Thermal conductivity κ vs. T. *(1)* Single crystal; *(2)* polycrystalline material [84K].

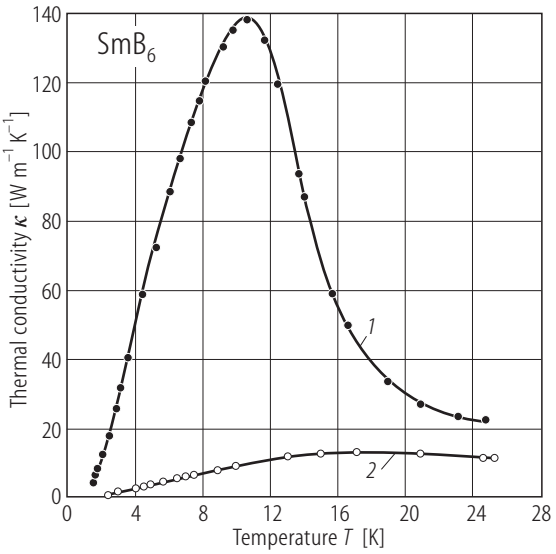

Fig. 39.

SmB_6. Heat capacity vs. temperature for two samples (dashed line: LaB_6 for comparison). Fig. b shows the low temperature range on an expanded scale [71N2].

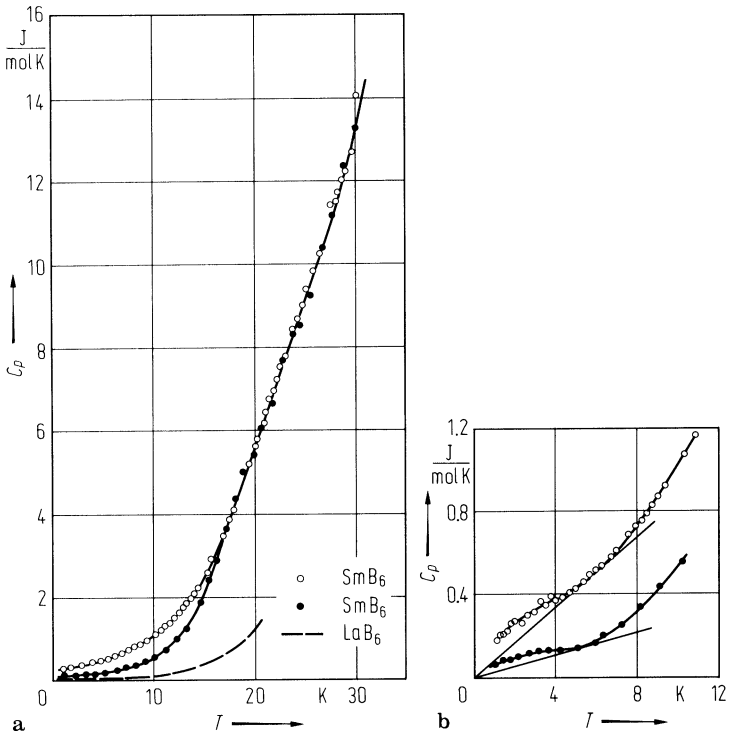

Fig. 40.

Metal hexaborides. Characteristic Einstein temperatures of the Ln atoms vs. atomic number of the Ln element; full circles [94K2]; triangles [99T].

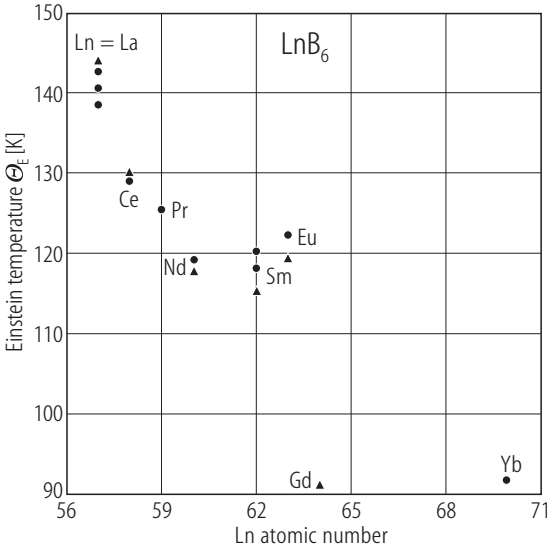

Fig. 41.

SmB_6. Neutron scattering. **(a)** $S(Q,E)$ at T = 20 K with E_0 = 60 meV for $<\Phi>$ = 5°, Q (14meV) = 0.80 Å^{-1}, **(b)** $<\Phi>$ = 11.5°, Q (14meV) = 1.21 Å^{-1}. $Q(E)$ is the momentum transfer at the energy transfer E. The beam time is 962 mkAh. Lines are the fits by Gaussians for phonons (at 10 and 25 meV) and Lorentzian at 14 meV. Horizontal bars indicating the FWHM of the instrumental energy resolution for corresponding energy transfer. Insert: integrated-intensity (cross section σ^t_m) Q-dependence for the 14 meV peak obtained from four detector groups $<\Phi>$ = 5°, 11.5°, 16.5°, 21.5° [93A2].

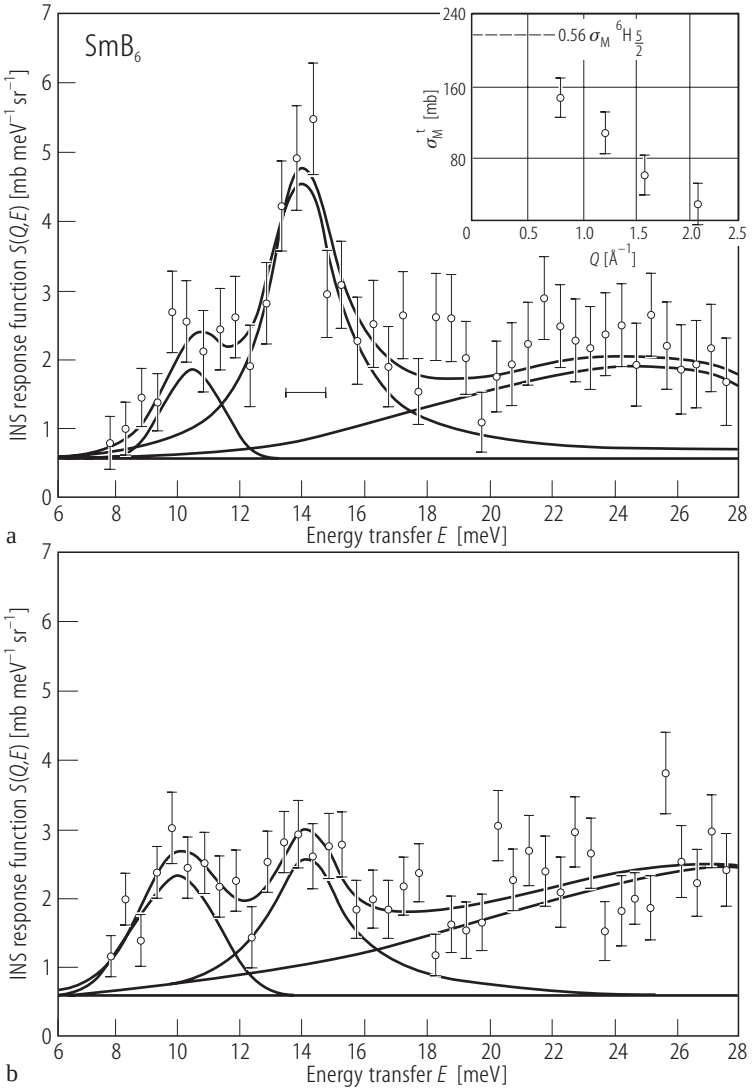

Fig. 42.

SmB_6. Neutron scattering. Magnetic contributions to $S(Q, \omega)$ at 20 K for $<\Phi> = 5°$ obtained from measurements with E_0 = 300 **(a)** and 200 meV **(b)** in CCR (closed-cycle refrigerator). Lines are the fit by Gaussians. $Q(E)$ is the momentum transfer at the energy transfer E. Horizontal bars indicating the FWHM of the instrumental energy resolution for corresponding energy transfer. Insert: calculated dynamical structure factors as functions of neutron momentum transfer for $^7F_0 \rightarrow {}^7F_1$ ($J = 0 \rightarrow 1$), and $^6H_{5/2} \rightarrow {}^6H_{7/2}$ ($J = 5/2 \rightarrow 7/2$) intermultiplet transitions [93A1].

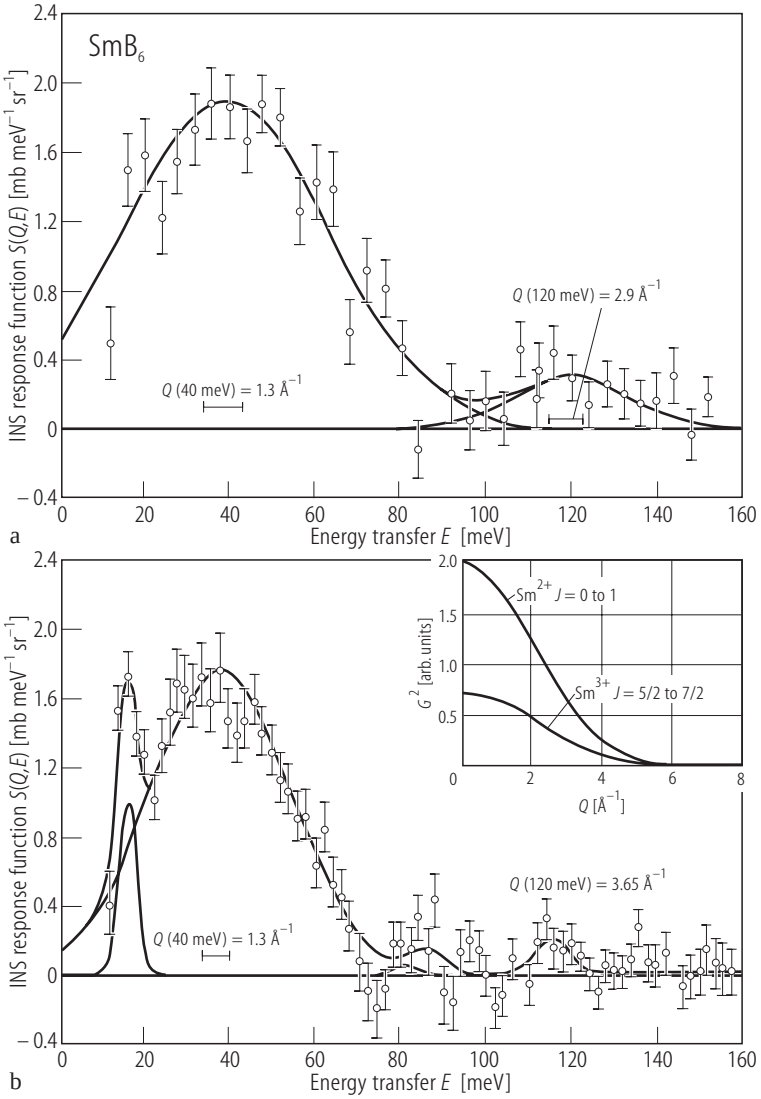

Fig. 43.

SmB_6. Calculated densities of d and f states g^d, g^f from the two-band Hubbard model with parabolic density of states for the d band. The bottom curve is for a filled non-degenerate f state with a gap to the d states and the upper curves represent partial f occupation $1 \leq n^f \leq 2$. The gap disappears for $n^d \approx 0.6$. The results are based on a solution of the single site coherent potential approximation in terms of the site Green's function. Parameters: $V/W = 0.05$ (V one electron matrix element, W = band width of the d band); $g = j = 0$ (g = direct Coulomb interaction, j = exchange interaction); n^d, n^f = occupation density of the d and f states [79M].

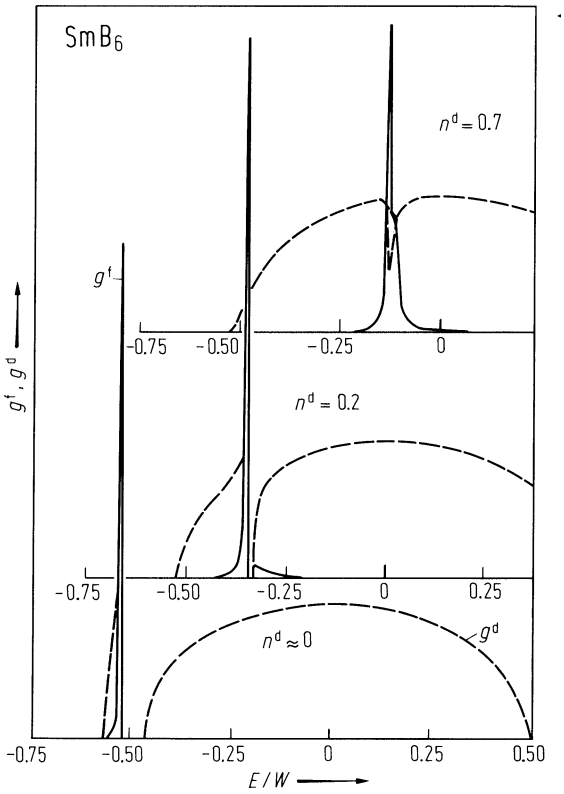

Fig. 44.

SmE_6. Molar susceptibility vs. temperature. Experimental data: [69M1]; theoretical fit: [71N2] (dashed curve: sum of the susceptibilities of the $4f^6$ and f^5s || configurations; dot - dashed curve: contribution due to the f^5s ⊥ term). χ_m in CGS units.